Development and Characterization of Ear-EEG for Real-Life Brain-Monitoring

Ph.D. Dissertation

Simon Lind Kappel

September, 2016

AARHUS
UNIVERSITY
DEPARTMENT OF ENGINEERING

Development and Characterization of Ear-EEG for Real-Life Brain-Monitoring

A Dissertation
Presented to the Faculty of Science and Technology
of Aarhus University
in Partial Fulfilment of the Requirements for the
PhD Degree

by

Simon Lind Kappel

supervised by

Preben Kidmose

September, 2016

Revised and published June, 2018
(Corrections and updates are listed on page 64 and 65)

ISBN: 978-87-7507-420-4
DOI: 10.7146/aul.260.183

Abstract

Functional brain monitoring methods for neuroscience and medical diagnostics have until recently been limited to laboratory settings. However, there is a great potential for studying the human brain in the everyday life, with measurements performed in more realistic real-life settings. Electroencephalography (EEG) can be measured in real-life using wearable EEG equipment. Current wearable EEG devices are typically based on scalp electrodes, causing the devices to be visible and often uncomfortable to wear for long-term recordings. Ear-EEG is a method where EEG is recorded from electrodes placed in the ear. The Ear-EEG supports non-invasive long-term recordings of EEG in real-life in a discreet way. This Ph.D. project concerns the characterization and development of ear-EEG for real-life brain-monitoring. This was addressed through characterization of physiological artifacts in real-life settings, development and characterization of dry-contact electrodes for real-life ear-EEG acquisition, measurements of ear-EEG in real-life, and development of a method for mapping cortical sources to the ear. Characterization of physiological artifacts showed a similar artifact level for recordings from ear electrodes and temporal lobe scalp electrodes. Dry-contact electrodes and flexible earpieces were developed to increase the comfort and user-friendliness of the ear-EEG. In addition, electronic instrumentation was developed to allow implementation in a hearing-aid-sized ear-EEG device. Ear-EEG measurements performed in real-life settings with the dry-contact electrodes, were comparable to temporal lobe scalp EEG, when referenced to a Cz scalp electrode. However, the recordings showed that further development of the earpieces and electrodes are needed to obtain a satisfying recording quality, when the reference is located close to or in the ear. Mapping of the electric fields from well-defined cortical sources to the ear, showed good agreement with previous ear-EEG studies and has the potential to provide valuable information for future development of the ear-EEG method. The Ph.D. project showed that ear-EEG measurements can be performed in real-life, with dry-contact electrodes. The brain processes studied, were established with comparable clarity on recordings from temporal lobe scalp and ear electrodes. With further development of the earpieces, electrodes, and electronic instrumentation, it appears to be realistic to implement ear-EEG into unobtrusive and user-friendly devices for monitoring of human brain processes in real-life.

Resumé

Funktionelle målemetoder, som anvendes til hjerneforskning og medicinsk diagnostik, har indtil for nylig været begrænset til laboratorier. Der er imidlertid et stort potentiale for at foretage hjerneforskning i hverdagen, hvor målinger kan foretages i mere realistiske omgivelser. Elektroencefalografi (EEG) kan måles i hverdagen vha. bærbart EEG udstyr. Nuværende bærbare EEG systemer er typisk baseret på hovedbundselektroder. Systemerne er derfor synlige og ofte ubehagelige at bære i længere tid. Øre-EEG er en metode, hvor EEG optages fra elektroder placeret i øret. Øre-EEG understøtter non-invasive langtidsmålinger af EEG i hverdagen på en diskret måde. Nærværende Ph.D. projekt omhandler karakterisering og udvikling af øre-EEG til monitorering af hjerneaktivitet i hverdagen. Dette blev adresseret gennem karakterisering af fysiologiske artefakter i hverdagssituationer, udvikling og karakterisering af tørelektroder til hverdagsmåling af øre-EEG, måling af øre-EEG i hverdagen og udvikling af en metode til at kortlægge de elektriske felters udbredelse fra kortikale kilder til øret. Karakterisering af fysiologiske artefakter viste et sammenligneligt artifaktniveau for optagelser fra øreelektroder og hovedbundselektroder over temporallappen. Der blev udviklet en ny tørelektrodeplatform og fleksible øreproppper, som øger komfort og brugervenlighed af øre-EEG. Derudover blev der udviklet elektrisk instrumentering, som understøtter implementering i et høreapparatlignende øre-EEG apparat. Målinger af øre-EEG foretaget med tørelektroderne i hverdagen var sammenlignelige med målinger fra hovedbundselektroder over temporallappen, når referenceelektroden var placeret i Cz positionen i hovedbunden. Målingerne viste imidlertid, at der er brug for yderligere udvikling af øreproppper og elektroder, for at opnå en tilfredsstillende målekvalitet, hvis referenceelektroden placeres tæt på eller i øret. Kortlægning af de elektriske felters udbredelse fra veldefinerede kortikale kilder til øret viste god overensstemmelse med tidligere øre-EEG studier, og har potentiale til at give værdifuld information til den videre udvikling af øre-EEG metoden. Ph.D. projektet viste at øre-EEG målinger kan foretages i hverdagen med tøreletroder. De processer i hjernen, som blev studeret, var synlige på målinger fra både temporale hovedbundselektroder og øreelektroder med lignende klarhed. Med yderligere udvikling af øreproppper, elektroder og den elektriske instrumentering ser det ud til at være realistisk at implementere øre-EEG i et diskret og brugervenligt apparat, som kan benyttes til monitorering af hjerne aktivitet i hverdagen.

Acknowledgements

This Ph.D. was supported by the Danish National Advanced Technology Foundation under the project title "Ear-EEG based hypoglycaemia alarm" (j.nr. 110-2013-1). I would like to thank Widex A/S and Hyposafe A/S for their collaboration and contribution to the Ph.D. A special thanks to Hans Olaf Toft, Mikael Andersen, Mike L. Rank, Søren Kilsgaard, and Erik S. Christensen for their contributions to the project and close collaboration.

Thank you to Scott Makeig and Swartz Center for Computational Neuroscience for inviting me to stay and learn from your expertise. I appreciate all the experience and knowledge you shared with me during my stay. Also thank you to Zeynep A. Acar, Yu-Te Wang, and Masaki Nakanishi for discussions and collaboration during the stay.

To my colleagues in the neurotechnology lab at Aarhus University, I owe you big thanks for fruitful discussions and collaboration. A special thank you to Xiong Zhou, Kaare B. Mikkelsen, and Christian B. Christensen for collaboration on several of the papers in this dissertation.

I would like to express my gratitude to my supervisor, Senior Associate Professor Preben Kidmose, for offering me the opportunity to pursue the Ph.D. Thank you for supporting me throughout the Ph.D. I am very grateful for all the hours you have spent supervising me. I have appreciated our discussions and have learned a lot from your experience and knowledge.

I also owe great thanks to my family for their support. Especially my loving wife, Michelle, who has supported me during the entire journey. Without her support, I would not have completed the journey. Thank you for encouraging me when I needed it, and challenging me when that was necessary.

Simon Lind Kappel
Aarhus, September 2016

Contents

Abstract i

Resumé ii

Acknowledgement iii

I Summary of work 1

1 Introduction 2
- 1.1 Motivation . . . 2
- 1.2 The hypoglycemia project . . . 4
- 1.3 Research objectives . . . 5
- 1.4 Stay abroad . . . 5
- 1.5 Scientific papers . . . 5

2 Background 7
- 2.1 Electroencephalography . . . 7
- 2.2 Electrode-skin interface . . . 9
- 2.3 Event-related potentials . . . 12
- 2.4 Spontaneous EEG . . . 14
- 2.5 Ear-EEG electrode labeling . . . 15

3 Characterization of physiological artifacts 16
- 3.1 Lab study of physiological artifacts . . . 16
- 3.2 Real-life study of artifacts . . . 20

4 Dry-contact ear-EEG 22
- 4.1 Ear-EEG electrodes . . . 22
- 4.2 Electrode-skin impedance . . . 24
- 4.3 Electronic instrumentation . . . 26

5 Real-life ear-EEG 32
- 5.1 Ear-EEG recordings . . . 33

5.2 Electrode configurations 36
5.3 Brain computer interface 39

6 Electric fields in the ear **41**
6.1 Ear-EEG forward model 42
6.2 Mapping cortical sources to the ear 45
6.3 Validation of the forward model 46

7 Conclusion and perspectives **49**
7.1 Conclusion 49
7.2 Perspectives 50

List of Abbreviations **52**

Bibliography **54**

Corrections and updates **64**

II Scientific papers **66**

P1 Physiological artifacts in scalp EEG and ear-EEG **67**

P2 Laboratory and Real-Life Dry-Contact Ear-EEG Recordings **68**

P3 Reference Configurations for Ear-EEG Steady-State Responses **70**

P4 Study of Impedance Spectra for Dry and Wet EarEEG Electrodes **71**

P5 A Method for Quantitative Assessment of Artifacts in EEG, and an ... **72**

P6 A study of real-life artifacts for scalp EEG and ear-EEG **73**

P7 A Wearable Ear-EEG Recording System Based on Dry-Contact Active ... **78**

P8 Developing an Online Steady-State Visual Evoked Potential-Based ... **79**

P9 EEG Recorded from the Ear: Characterizing the Ear-EEG Method **80**

Part I

Summary of work

Chapter 1

Introduction

"As humans, we can identify galaxies light years away, we can study particles smaller than an atom. But we still haven't unlocked the mystery of the three pounds of matter that sits between our ears."
— Barack Obama, President of the USA, 2013

1.1 Motivation

In recent years, the scientific as well as the public interest in neuroscience has increased rapidly. One example of this trend is the initiation of big research projects like the European Human Brain Project[1] and the American BRAIN Initiative[2].
The human brain has always been a mystery for human kind. However, within the last century research has come far in understanding the structure and function of the human brain. This has been accomplished through the development of new methods to measure the human brain activity. Current non-invasive methods include functional magnetic resonance imaging (fMRI), functional near-infrared spectroscopy (fNIRS), positron emission tomography (PET), single-photon emission computed tomography (SPECT), magnetoencephalography (MEG) and electroencephalography (EEG) [39, 92, 64]. Studies of brain activity are usually performed in a laboratory setting. For the majority of the available methods a laboratory is required, because the measurements rely on big machines taking up the space of a dedicated room in a hospital. In addition, interference in terms of noise and artifacts can better be controlled in a laboratory setting. However, recordings of both fNIRS and EEG can also be performed outside the constraints of a laboratory,

[1] The European Human Brain Project was started in October 2013 with a budget of about 1000 million Euros. For more information visit www.humanbrainproject.eu.

[2] The American BRAIN initiative was announced by Barack Obama in April 2013 with a budget of about 110 million US Dollars. For more information visit www.braininitiative.nih.gov.

and have the potential to be used for real-life monitoring in everyday life [22, 81]. Even though fNIRS is an interesting method, it does not fall within the scope of this Ph.D. and will not be covered in this dissertation.

EEG is a method for non-invasive recording of skin potentials, which represents aggregated electrical activity in the brain from populations of temporally synchronized and spatially aligned neurons. The main clinical applications of EEG include sleep monitoring [85, 52], screening of auditory nerve and brainstem lesions [75], objective hearing assessment [61, 84], epilepsy [44, 36], analysis of coma patients [103], and determination of brain death [49]. Other applications explored in research, include brain computer interface (BCI) [38, 100], diagnostics and monitoring of mental diseases [73, 97], and investigation of visual function [67, 59].
Conventionally, EEG is measured with a full cap system in a controlled laboratory environment, as shown in Figure 1.1(a). However, for e.g. sleep monitoring, the recordings can be performed at home with an ambulatory EEG system, which is typically based on a conventional EEG cap connected to a portable EEG amplifier, as shown in Figure 1.1(b). There is currently a lot of focus on the development of user-friendly wearable EEG systems, enabling monitoring of EEG in real-life environments [22]. The emergence of wearable EEG has the potential to open up new fields of applications and research.

Ear-EEG is an EEG recording method, where electrodes are placed in the ear, as shown in Figure 1.1(c). The ear-EEG methodology has been pioneered in collaboration between Preben Kidmose's group at Department of Engineering, Aarhus University, Danilo P. Mandic's group at Imperial College London, and the hearing aid manufacturer Widex A/S [62, 55].
Ear-EEG addresses the practical challenges of non-invasive and robust EEG acquisition in real-life environments. The shape of ear-EEG devices is similar to the earpieces used for hearing aids and provides a discreet and comfortable way of recording EEG. Thus, a wearable EEG device, based on ear-EEG, could be used for

(a) Laboratory EEG (b) Ambulatory EEG (c) Ear-EEG

Figure 1.1: The evolution of EEG systems from conventional scalp EEG (a) to ambulatory (b) and wearable ear-EEG (c)

monitoring of EEG for several days [62]. The ear-EEG has been validated through laboratory studies of event related EEG potentials [55, 62]. However, the vision is also to use the ear-EEG for real-life acquisition of spontaneous EEG. The ear-EEG could most likely be utilized for the majority of the clinical and research applications mentioned above. This includes more specific applications, such as sleep diagnostics [106], monitoring of impending severe hypoglycemia (SH, insulin shock) in insulin-treated diabetics [53] and monitoring of frequency and length of seizures in childhood absence epilepsy [36]. Studies show that impending SH can be observed in the EEG, and a device enabling constant monitoring of EEG in the everyday life could effectively alarm about an impending SH [53, 93].

1.2 The hypoglycemia project

This Ph.D. project was part of a bigger project, funded by the Innovation foundation[3]. The project was initiated in September 2013 and scheduled to end in September 2017. It is a collaboration between Aarhus University, Widex A/S, Odense University Hospital and Hyposafe A/S. The main objective of the project is to develop a device prototype, based on dry-contact electrode technology, which enables measurements of EEG in real-life environments, using the ear-EEG technology. The goal is to obtain a recording quality which enables detection of SH. A substantial proportion of patients with insulin treated diabetes experience complications with SH, and an even bigger group of diabetes patients live with a constant fear of SH [53]. It is the vision of the project to develop a device, based on ear-EEG, which can warn diabetics about impending SH and enable the user to act accordingly. Detection of SH is a convenient application, because it is medical, but not diagnostic, thus the regulatory approvals of the device are less complex.
The development of the device prototype involves three major scientific tasks:

1. The development of dry-contact electrodes for recording of real-life ear-EEG.
2. The development of electronic instrumentation optimized for ear-EEG.
3. Characterization of ear-EEG in real-life settings, based on well-established EEG paradigms.

The first step in validating ear-EEG for detection of SH, is to perform recordings of induced SH in a controlled hospital setting. These recordings are dependent on a stable device prototype, and are scheduled to be carried out at the end of the hypoglycemia project, and therefore not within the time-frame of this Ph.D.

[3]The former Danish national advanced technology foundation, j.nr. 110-2013-1

1.3 Research objectives

As part of the hypoglycemia project, the main focus of the Ph.D. project was the development of dry-contact electrode technology for recording of real-life ear-EEG and the characterization of ear-EEG in real-life settings, based on well-established EEG paradigms. This was formulated in a central research question:

"Previous studies have shown that recordings from ear-EEG and temporal lobe scalp EEG carries similar information about brain processes - can similar results be obtained in real-life settings, for recordings performed with dry-contact electrodes?"

The research question was addressed through four research objectives, aiming to clarify the research tasks needed to answer the question.

1. Characterization of real-life physiological artifacts.
2. Development and characterization of dry-contact electrodes for ear-EEG.
3. Characterization of ear-EEG based on well-established EEG paradigms in real-life settings.
4. Development of a method for mapping cortical sources to the ear.

1.4 Stay abroad

From January to June 2015 I visited Swartz Center for Computational Neuroscience (SCCN), University of California San Diego, USA. SCCN is directed by Scott Makeig, who is one of the pioneers of EEG analysis using independent component analysis (ICA) [69]. EEGlab was developed at SCCN and is a widely used Matlab toolbox for analysis of EEG data [34]. The main focus of the stay was the acquisition of high density EEG data and the development of realistic head models for mapping cortical sources to the ear. The data acquired during the stay have not yet been analyzed, and are therefore not treated in this dissertation.

1.5 Scientific papers

The research conducted in the Ph.D. is described in a series of scientific papers. The core papers present research performed to address the research objectives described in Section 1.3. The remaining joined project papers are more loosely related to the research objectives.

1.5.1 Core papers used within the dissertation

P1 S. L. Kappel, D. Looney, D. P. Mandic, and P. Kidmose. "Physiological artifacts in scalp EEG and ear-EEG". in: *Biomedical Engineering Online* 16.1 (Aug. 2017), p. 103. DOI: 10.1186/s12938-017-0391-2

P2 a) S. L. Kappel, M. L. Rank, H. O. Toft, M. Andersen, and P. Kidmose. "Dry-Contact Electrode Ear-EEG". in: *IEEE Trans Biomed Eng* (May 2018). DOI: 10.1109/TBME.2018.2835778;
b) S. L. Kappel and P. Kidmose. "Real-Life Dry-Contact Ear-EEG". in: *Int. Conf. of the IEEE Engineering in Medicine and Biology Society (EMBC)* (July 2018)

P3 S. L. Kappel, C. B. Christensen, K. B. Mikkelsen, and P. Kidmose. "Reference Configurations for Ear-EEG Steady-State Responses". In: *Int. Conf. of the IEEE Engineering in Medicine and Biology Society (EMBC)* (2016). DOI: 10.1109/EMBC.2016.7592018

P4 S. L. Kappel and P. Kidmose. "Study of Impedance Spectra for Dry and Wet EarEEG Electrodes". In: *Int. Conf. of the IEEE Engineering in Medicine and Biology Society (EMBC)* (2015), pp. 3161–3164. DOI: 10.1109/EMBC.2015.7319063

P5 S. L. Kappel, D. Looney, D. P. Mandic, and P. Kidmose. "A Method for Quantitative Assessment of Artifacts in EEG, and an Empirical Study of Artifacts". In: *Int. Conf. of the IEEE Engineering in Medicine and Biology Society (EMBC)* (2014), pp. 1686–1690. DOI: 10.1109/EMBC.2014.6943931

P6 S. L. Kappel and P. Kidmose. "A study of real-life artifacts for scalp EEG and ear-EEG". in: *unpublished* (2016)

1.5.2 Joined project papers

P7 X. Zhou, Q. Li, S. Kilsgaard, F. Moradi, S. L. Kappel, and P. Kidmose. "A Wearable Ear-EEG Recording System Based on Dry-Contact Active Electrodes". In: *Symposia on VLSI Technology and Circuits* (June 2016). DOI: 10.1109/VLSIC.2016.7573559

P8 Y. T. Wang, M. Nakanishi, S. L. Kappel, P. Kidmose, D. P. Mandic, Y. Wang, CK. Cheng, and TP. Jung. "Developing an Online Steady-State Visual Evoked Potential-Based Brain-Computer Interface System Using EarEEG". in: *Int. Conf. of the IEEE Engineering in Medicine and Biology Society (EMBC)* (2015), pp. 2271–2274. DOI: 10.1109/EMBC.2015.7318845

P9 K. B. Mikkelsen, S. L. Kappel, D. P. Mandic, and P. Kidmose. "EEG Recorded from the Ear: Characterizing the Ear-EEG Method". In: *Frontiers in Neuroscience* 9 (Nov. 2015), pp. 1–8. DOI: 10.3389/fnins.2015.00438

Chapter 2

Background

This chapter introduces concepts and terms that will be used throughout the dissertation. The chapter is divided in five Sections: 2.1 introduce basic neuroanatomy and the origin of EEG, 2.2 outline the electrochemical processes in the electrode-skin interface, 2.3 presents the concept of EEG potentials arising from well-defined events, 2.4 introduce the spontaneous EEG, and 2.5 outline the labeling convention used for ear-EEG electrodes.

2.1 Electroencephalography

Electroencephalography (EEG) is a method for monitoring the electrical activity in the brain, through measurements of the electrical skin potentials on the scalp. The first human EEG recordings were performed in 1924 by Hans Berger, who reported the temporal development of skin potentials measured on the scalp [16, 63]. The EEG recordings performed by Hans Berger showed oscillations in the clinical alpha frequency band (8-12 Hz).

2.1.1 Source of the EEG

The brain can be divided in three main regions; the brainstem, cerebellum and cerebrum. The EEG primarily originates from the outer layer of the cerebrum, which is called the cerebral cortex. The cerebral cortex can be further divided in 4 lobes, as illustrated in Figure 2.1. The lobes of particular interest for the current project are the temporal lobes, where the primary auditory cortices are located, and the occipital lobe, where the primary visual cortices are located [91].

The most developed part of the brain is the neocortex, which occupy the majority of the cerebral cortex. The human neocortex can generally be arranged in 6 layers containing two main types of neurons; pyramidal and non-pyramidal neurons [26]. Pyramidal neurons stretches across all layers, with their cell bodies primarily located in layer II and V [91]. They are characterized by a triangular shaped cell

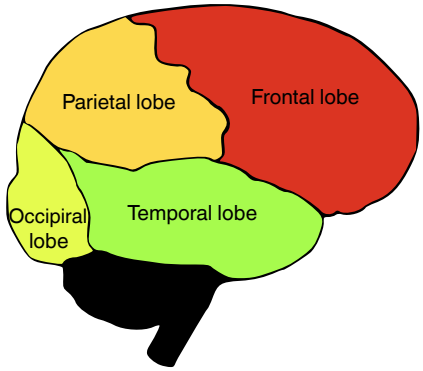

Figure 2.1: Illustration of the lobes of the cerebral cortex. [Source: modified from Wikipedia]

body and usually have a long dendritic tree extending toward the cortical surface as illustrated in Figure 2.2(a). In addition, pyramidal neurons are characterized by spatial alignment in the cortex as illustrated in Figure 2.2(b). Non-pyramidal neurons are remarkably different from pyramidal neurons. They have a small cell body and their dendrites spring in all directions [26].
Each neuron in the brain is connected to thousands of other neurons through chemical synapses. A synapse is formed between the axon of a neuron and a synaptic ending on a dendrite of another neuron [91]. An action potential in the axon cause

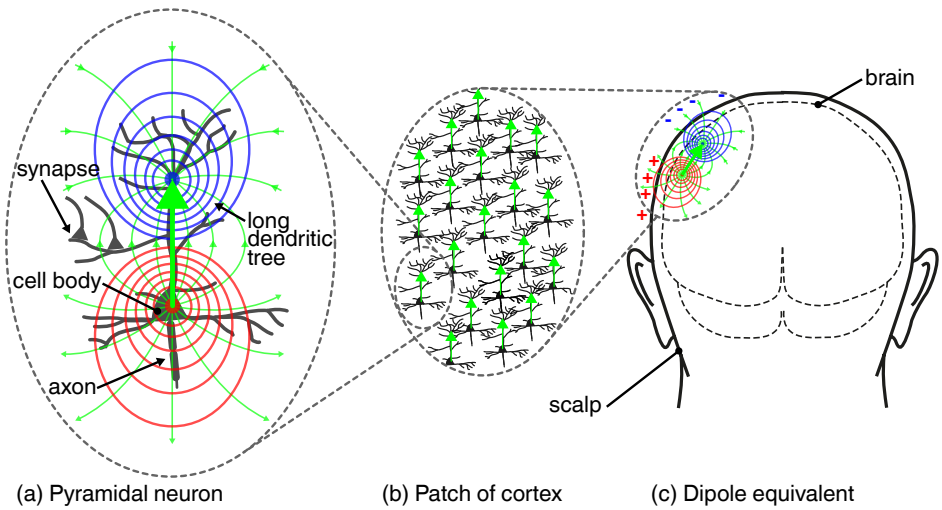

Figure 2.2: (a) Pyramidal neuron, with illustration of current (green) and equipotential lines (blue/red) for synchronous activation of excitatory synapses on the long dendritic tree. (b) Pyramidal neurons in a patch of cortex. The patch also contains other types of neurons, but here only the pyramidal neurons are illustrated. (c) Dipole equivalent formed by thousands of spatially aligned and temporally synchronized pyramidal neurons.

the presynaptic terminal to release neurotransmitters, which open ion-channels for positive (excitatory) or negative (inhibitory) charged ions in the postsynaptic terminal. This results in an increased flux of ions in the postsynaptic terminal, which cause an extracellular ion-current around the dendrite, where the active synaptic terminal is located. If numerous excitatory synapses on the long dendritic tree of a pyramidal neuron are synchronously active, the neuron can be regarded as a current dipole with a source (+) around the cell body and a sink (-) around the long dendritic tree, as illustrated in Figure 2.2(a). The dipole equivalent formed by a single neuron is not enough to create measurable changes in the scalp potential. Thus, the EEG observed on the scalp originate from thousands of spatially aligned and temporally synchronized neurons, which can be equated by a single current dipole from the macroscopic view where the EEG is measured, as illustrated in Figure 2.2(c).

The EEG is conventionally measured by electrodes placed on the scalp. The electrodes are typically located according to standard location systems like the 10-20 system [26].

2.2 Electrode-skin interface

The electrode forms the transducer between the skin and the analog front-end, converting ion-based charge transport in the body into electron-based charge transport in the electrode and electronics. This conversion takes place in the electrode-electrolyte interface, where the electrolyte consists of perspiration from the skin and electrode gel.

2.2.1 Half-cell potential

The half-cell potential is the potential difference between the electrolyte and electrode in an electrochemical half-cell. The half-cell potential is mainly determined by the electrode material, temperature, and concentration of ions of the electrode material in the electrolyte [76]. The half-cell potential arises from chemical reactions in the double-layer between the electrode and electrolyte, as illustrated on

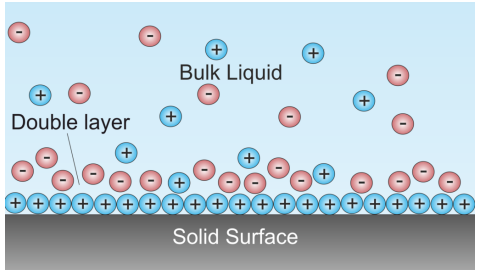

Figure 2.3: Illustration of the double-layer formed between a metal and an electrolyte. [Source: modified from Wikipedia]

Figure 2.3. For metal electrodes, the double-layer is formed by cations on the surface of the electrode and anions in the electrolyte which are electrostatically attracted to the cations. [42]. The double-layer is typically a few nanometer thick and acts as a capacitive interface between the electrode and electrolyte.

The half-cell potential reflects an equilibrium of the chemical reactions in the double-layer. The time it takes for this equilibrium to be established is determined by the electrode material. Until the equilibrium has been established, the half-cell potential will be changing and create noise in the recordings. Practical experience show that the potential over the electrode-skin interface usually stabilize within a few minutes [51]. If the double-layer is disturbed, by e.g. motion, the equilibrium will have to be reestablished.

Electrode materials can be arranged in polarizable and non-polarizable electrodes, determined by the dominating characteristics of their interface with an electrolyte. However, the characteristics of a few coatings fall within a third group termed pseudocapacitive electrodes. The characteristics related to the different electrode types are outlined below.

2.2.2 Polarizable electrode

For an ideal polarizable (capacitive) electrode, no actual charge is flowing in the electrode-electrolyte interface, when a current is applied [76]. The current will be a displacement current, caused by changes in the concentration of ions at the interface. This means that the charge storage for a polarizable electrode is electrostatic [20]. Thus, a polarizable electrode acts as a capacitive interface, where a change in the charge, ΔQ, stored at the interface is proportional to a change in the voltage, ΔV, over the interface

$$\Delta Q = \Delta V \cdot C \tag{2.1}$$

where C is the capacitance in farads, ΔQ is in coulombs and ΔV is in volts.
Perfectly polarizable electrodes cannot be fabricated, but a relatively inert metal like platinum (Pb) approaches a perfectly polarizable electrode quite well.

2.2.3 Non-polarizable electrode

An ideal non-polarizable electrode is characterized by easy charge transport across the electrode-electrolyte interface, causing an applied current to be purely faradaic [76]. This faradaic current is based on oxidation and reduction of the metal. A silver-silver chloride (Ag/AgCl) electrode is a good example of a practical electrode which approached the characteristics of a non-polarizable electrode.

2.2.4 Pseudocapacitive electrodes

A pseudocapacitive electrode is a material with the electrochemical signature of a polarizable (capacitive) electrode, but where charge is not stored electrostatically. Instead charge transfer in a pseudocapacitive interface is due to fast and reversible faradeic redox reactions on the surface of the electrode [13, 42]. Thus, pseudocapacitance originate from electron charge-transfer through changes in the oxidation state of the electrode material, and corresponding insertion (electrosorption) of ions from the electrolyte, which has pervaded the double-layer [20, 27]. This means that no ions of the electrode material is released to the electrolyte.
For some electrode materials pseudocapacitance is the dominating method of charge transfer and the pseudocapacitance is much higher than the double-layer capacitance [30]. This is the case for coatings like ruthenium oxide (RuO_2) and iridium-oxide (IrO_2) [29].

2.2.5 EEG electrodes

Conventional laboratory EEG recordings are typically performed with wet Ag/AgCl electrodes, where an electrode gel is applied between the electrode and skin. The electrode gel is usually a solution with ionic concentrations higher than the extracellular fluid in the human body. The electrode gel improves the ion transport between the skin and the electrode. One of the arguments for the extensive use of Ag/AgCl electrodes is that the potential over the electrode-skin interface stabilizes within a few minutes, enabling low noise recordings shortly after application of the electrode [51]. For a lab environment, the application of gel between the electrode and skin is normally not a problem. However, for wearable EEG, great advantages, in terms on mounting time and user-friendliness, can be obtained by using dry-contact electrodes, where no electrode gel is applied. However, dry-contact electrodes impose new challenges that must be addressed to obtain a satisfying recording quality.

For dry-contact electrodes, the electrolyte in the electrode-skin interface will primarily be formed by perspiration from the skin. Thus, the amount of electrolyte will typically be quite limited, and the double-layer in the electrode-skin interface can easily be disturbed by motion. Disturbance of the double-layer will change the half-cell potential and capacitance of the electrode-skin interface. In addition, motion will alter the geometrical area between the electrode and skin, which also change the capacitance of the interface. These aspects contribute to a higher and more varying impedance of the electrode-skin interface for dry-contact electrodes, compared to wet electrodes [23]. Thus, in order to measure EEG with dry-contact electrodes, the electronic instrumentation must be designed to accommodate these higher and more varying impedances [94]. The impedance of the electrode-skin interface can often be reduced by increasing the surface area of the electrode. However, there is typically a trade-off between the size of the electrodes and the distance

between the electrodes. In order to achieve a better trade-off, a nanostructured surface coating can be utilized to increase the surface area of the electrode without increasing the size of the electrode [27].

2.3 Event-related potentials

An event-related potential (ERP) is an electrical potential in the body arising as a result of a specific event. ERPs can be measured within all of the human nervous system, but the term is usually used, and will also be used here, to refer to the EEG potentials related to an event. The ERP is the difference between the spontaneous EEG potential and the potential related to the event. ERPs can be divided in to two main groups; steady-state ERPs and transient ERPs. The potentials can be evoked by stimulation of all of our senses; e.g. auditory evoked potentials (AEPs), visual evoked potentials (VEPs) and somatosensory evoked potentials (SEPs). For ear-EEG, auditory paradigms are especially interesting because of the ears' location in the vicinity of the auditory nerve and primary auditory cortices [90]. Additionally, a loudspeaker can easily be integrated with an ear-EEG earpiece, enabling the development of a single device to perform both stimulation and recording of the response.

The amplitude of the ERP is typically small compared to the noise level of the recording, and in order to interpretate the ERP, the noise must be attenuated. For ERP recordings, the noise contributors include the spontaneous EEG, physiological artifacts, motion artifacts and electrical interference.

2.3.1 Time domain averaging

Typically the event, which causes the ERP, is repeated several times to enable time domain averaging (TDA) of the response. TDA attenuates the noise, while maintaining the power of the ERP.
The benefit of TDA can be illustrated by an EEG signal, $x(n)$, which is a sum of a deterministic signal, $d(n)$, corresponding to the ERP, and noise, $e(n)$, from the sources described above.

$$x(n) = d(n) + e(n) \tag{2.2}$$

where x(n) have $N, n = 0, \dots, N-1$, samples.
The TDA is calculated as the average over segments, each time-locked to the time of the events under study. $x_s(m)$ is the s'th segment extracted from $x(n)$ having M, $m = 0, \dots, M-1$, samples. Thus, the TDA, $\bar{x}(m)$, of S segments is defined by

$$\bar{x}(m) = \frac{1}{S}\sum_{s=0}^{S-1} x_s(m) \qquad . \tag{2.3}$$

Assume that the noise has zero mean, is uncorrelated between segments, and that the variance of the noise in all segments are equal ($\sigma_{x_1}^2 = \sigma_{x_s}^2$). The variance of the

noise will then decrease by a factor S [66], which can be expressed as

$$\sigma_{\bar{x}}^2 = \frac{\sigma_{x_s}^2}{S} \quad . \tag{2.4}$$

The deterministic signal will be unaffected by the averaging, resulting in a 3 dB improvement of the signal-to-noise ratio (SNR) when the number of segments is doubled. This generalizes to an SNR improvement of $10\log_{10}(S)$.
For practical EEG recordings the ERP will not be identical for each repetition of the stimulus, causing the SNR improvement to be lower than given above.

2.3.2 Steady-state ERPs

A steady-state response is an ERP evoked by a periodic repetition of a stimulus [86]. The periodic structure of the stimulus will also be present in the EEG, and makes it convenient to perform spectral analysis of the response. The analysis can be performed using e.g. Bartlett or Welch estimation of the power spectrum, however none of these methods include the phase information in the averaging. In order to obtain the SNR improvement described in Section 2.3.1, the phase information must be included in the averaging. This can be done by first performing TDA and then spectral analysis of the averaged response.

Steady-state responses can be measured from all of our senses, however for ear-EEG the auditory steady-state response (ASSR) is of particular interest. The ASSR is present in all of the auditory pathway, with cortical responses primarily evoked by repetition frequencies from 10 to 70 Hz, and brainstem responses evoked by repetition frequencies up to about 1000 Hz [80]. Applications of ASSR include objective hearing assessment [61, 84] and depth of anesthesia [82]. The "40 Hz auditory potential" is the most easily elicited ASSR and was first characterized by Galambos et al. in 1981 [43]. The ASSR evoked by white noise amplitude modulated with 40 Hz are well recognized in ear-EEG recordings [55, 62]. The 40 Hz ASSR is a cortical response largely unaffected by attention and cognitive processes, which is convenient for validation of ear-EEG [60].

A steady-state response can also be evoked by a repetitive visual stimuli, referred to as the steady-state visual evoked potential (SSVEP). The SSVEP stimulus can be presented in different ways, including areas flickering on a monitor [P8], flickering LEDs [62], and modulating of the ambient light [P2]. The strongest SSVEP has been reported for stimulus repetition frequencies from 6 to 15 Hz [15, 95]. Applications of SSVEP include assessment of visual function [59] and research within mental disorders like schizophrenia, autism, depression and anxiety [97]. Recent years SSVEP has also been used for BCI, because of the high accuracy and information transfer rate (ITR) that can be obtained with SSVEP based BCI systems [98, 100].

2.3.3 Transient ERPs

Transient ERPs are evoked by discrete events, typically with a random stimulus-onset asynchrony (SOA) to prevent oscillations in the clinical alpha band (8-12 Hz) and other periodic signal from becoming time-locked to the stimuli [68]. Analysis of transient ERPs are typically performed by TDA time-locked to the beginning of the events. Applications of transient ERPs include research within psychiatry [73], BCI [38, 31], auditory function [21] and visual function [67].
The auditory onset response is a well-characterized transient ERP [71]. Figure 2.4 show a sketch of a typical auditory onset response, evoked by an auditory cue presented to the subject with random SOA. The response is characterized by three distinct peaks; P1, N1, and P2 [71, 83]. Similar auditory onset responses has been measured with ear-EEG by Kidmose et al., 2013 [55].

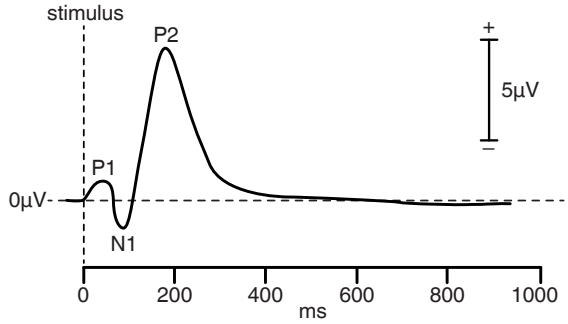

Figure 2.4: Sketch of a typical auditory onset response.

2.4 Spontaneous EEG

The spontaneous EEG is characterized by not being related to known events. Studies of the spontaneous EEG are particularly interesting in real-life settings, where the environment cannot be controlled, and human reactions to everyday life stimuli can be explored. However, analysis of the spontaneous EEG is often quite complex, compared to analysis of ERPs. This is partly because the EEG of interest is not time-locked to known events, which makes it difficult to perform TDA to improve the SNR of the data. In addition, the raw EEG is often difficult to interpret [63].

A well-known example of spontaneous EEG is alpha (8-12 Hz) oscillations in the occipital lobe. The highest power of these alpha oscillations are observed when the subject is awake and have closed eyes [26, 70]. Figure 2.5 shows a typical example of a power spectrum (left) and spectrogram (right) for an open/closed eyes experiment, measured with an electrode located over the parietal lobe. The power spectrum and spectrogram display a significantly increased alpha power in the closed eyes intervals of the recording. Another example of spontaneous EEG is sleep events like sleep spindles and K-complexes, which are well defined waveforms present during sleep [52].

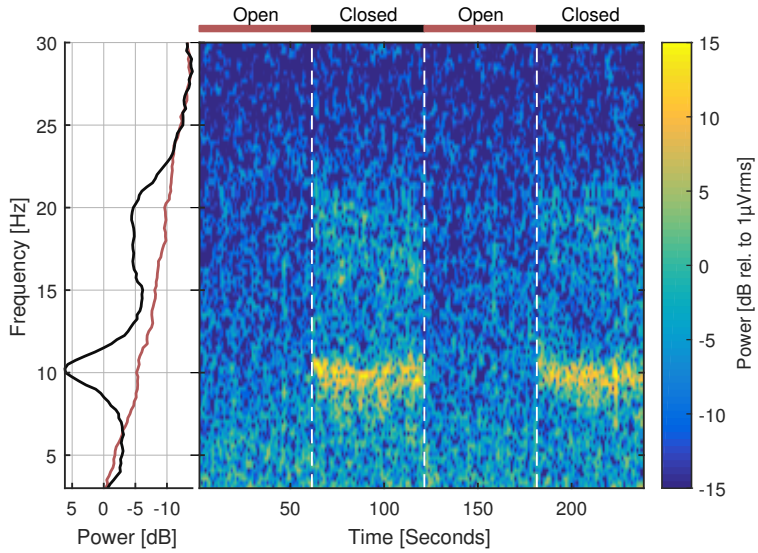

Figure 2.5: Power spectrum (left) and spectrogram (right) for an open/closed eyes experiment measured from a P3 electrode referenced a Cz electrode. The subject condition (open or closed eyes) is indicated above the spectrogram. The power spectrum is plotted for the open-eyes condition (red line) and the closed-eyes condition (black line) respectively.

2.5 Ear-EEG electrode labeling

The electrodes on the ear-EEG earpiece are labeled according to their anatomical position when the earpiece is placed in the ear. Figure 2.6 illustrate the label convention, which is "Exy", where "x" denotes the left (L) or right (R) ear, and "y" the position in the ear. Electrodes in the concha part of the ear have position labels "A", "B" and "C". The ear-lobe is position D and electrodes in the ear-canal have position labels "E" to "L". The labeling convention was defined by Kidmose et al. [55].

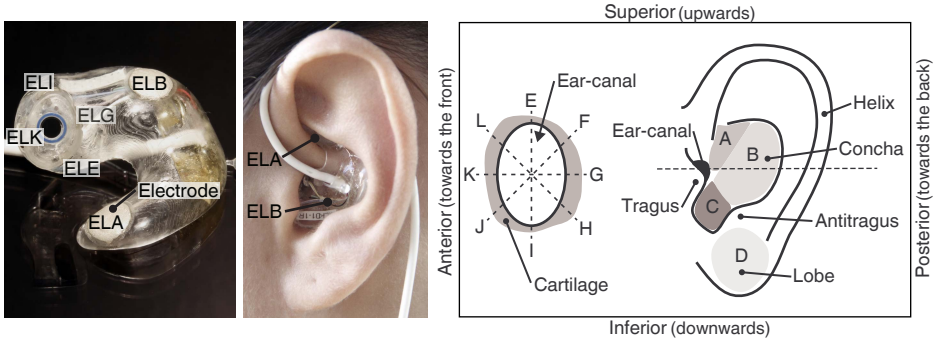

Figure 2.6: Left: ear-EEG earpiece with indication of electrode labels. middle: The earpiece inserted into the ear, with indication of two electrodes in the concha part of the ear. right: Sketches illustrating the ear-EEG electrode labeling convention.

Chapter 3

Characterization of physiological artifacts

Interference in terms of noise and artifacts is an inherent problem when recording EEG. In a lab environment artifacts and interference can largely be avoided or controlled, but in unrestrained real-life scenarios this is not possible. Physiological artifacts are defined as a category of artifacts with physiological origin, in contrast to artifacts related to motion or electrical interference. The most significant sources of physiological artifacts are eye blinks, eye movements, and muscle activity [65]. Characterization of how physiological artifacts contaminate the ear-EEG are particularly interesting, because this category of artifacts cannot be diminished by improving the design of the earpiece or electronic instrumentation, as opposed to artifact sources like motion and electrical interference.

The chapter is organized in Section 3.1, which summarize a study of real-life artifacts generated in a controlled lab environment, and Section 3.2, which presents a study of artifacts for different real-life settings outside the lab.
All recording presented in this chapter were performed with wet ear electrodes, to ensure that artifacts related to the electrode-skin interface had minimal influence on the characterization of physiological artifacts.

3.1 Lab study of physiological artifacts

The laboratory study of artifacts focused on characterizing real-life physiological artifacts generated in a controlled laboratory setting, where artifact sources could be studied separately. The study was divided in to two papers, with paper P5 establishing and validating a method for quantitative assessment of artifacts, and paper P1 presenting a study of physiological artifacts for 9 subjects.

The method for quantitative assessment of artifacts was based on measuring a steady-state response (SSR) in a relaxed condition with low levels of noise and artifact, and then compare the SNR of this response to the SNR of a SSR recorded

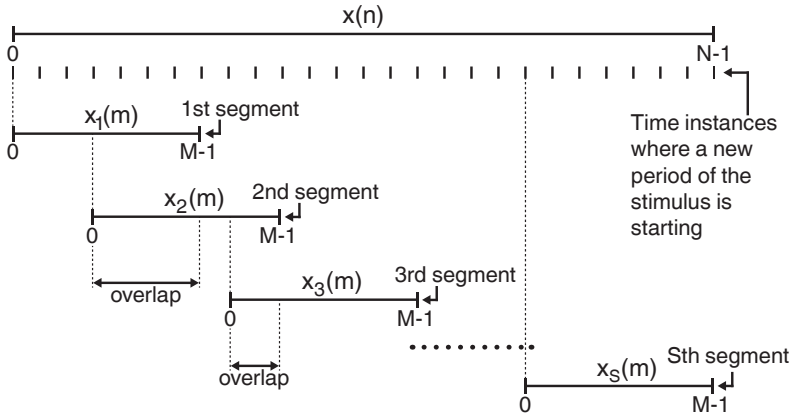

Figure 3.1: Each segment, $x_s(m)$, of length M is extracted from $x(n)$. To maintain correct phase of the SSR, each segment is aligned to the time when a new period of the stimulus begins. The overlap between the segments is randomly chosen between some user defined limits. [Figure and caption from [P1]]

in a condition influenced by artifacts [P5]. Thus, for each artifact under study, the method required SSR recordings in both the relaxed and artifact condition. This caused the duration of the paradigm, comprising several artifact conditions, to become critical.

Analysis of the SSRs was based on performing TDA, and then spectral analysis of the time averaged signal, as described in Section 2.3. In order to handle challenges with the duration of the paradigm, a novel method was proposed to reduce the recording time, while maintaining the resolution and number of segments in the TDA [P1]. The method relax the trade-off between spectral resolution and the number of segments, by allowing segments to overlap. Similarities can be drawn to the Welch method for power spectrum estimation, except that TDA is performed in the time-domain instead of the frequency-domain. An unintended drawback of overlapping is that it introduces a false periodicity in the averaged signal. By selecting the overlap randomly between some limits, this effect can be reduced. To avoid larger overlaps, the upper limit must be chosen with care. The segmentation with random overlap is illustrated in Figure 3.1, where S segments, $x_s(m)$, of length M are extracted from the recorded EEG signal, $x(n)$. To ensure a similar phase of the SSR in all segments, each segment must be aligned to the time instances where a new period of the stimulus begins. Paper P1 describes the method in detail and presents a simulation showing how the during of a SSR recording can be reduced, without decrease in the SNR of the SSR.

Paper P1 presents a characterization study of 8 real-life artifacts, generated in a lab environment, for 9 subjects. The artifacts were quantified by applying the methods described above to recordings of the ASSR. Recordings were also acquired in a relaxed condition for comparison. The conditions in the paradigm were:

1. **Relaxed**: Relax in a comfortable chair.
2. **Jaw clenching**: Clenching of the jaw with maximal strength.
3. **Ctrl. jaw move**: Jaw movements controlled by a custom made device [P5].
4. **Biting**: Biting around the custom made device [P5].
5. **Eye-blinking**: Eye-blinking with intervals of 1 s.

6.&7. **Horz./Vert. eye move**: Eye movements with the head fixed on a chin rest.

8.&9. **Horz./Vert. head move**: Head movements with restricted field of view and eyes fixed on a dot.

Figure 3.2 shows time domain examples of EEG recordings from a single subject in the relaxed, jaw clenching and eye-blinking conditions. The first row shows ear-EEG recordings from the ELK electrode referenced to the ELB electrode, the second row is recordings from the TP9 mastoid electrode referenced to the Cz electrode and the third row displays EEG data from the frontal F7 electrode referenced to the Cz electrode. An amplitude difference of approximate 20 dB was observed between the ear and scalp electrodes. However, the proportional increase in the noise level caused by e.g. jaw-clenching was similar for scalp and ear-EEG. Eye-blinking was very pronounced in the frontal scalp electrode, less visible in TP9, and even less visible in the ear-EEG electrode. This is consistent with our general experience of eye-blinking artifacts in ear-EEG [P1].

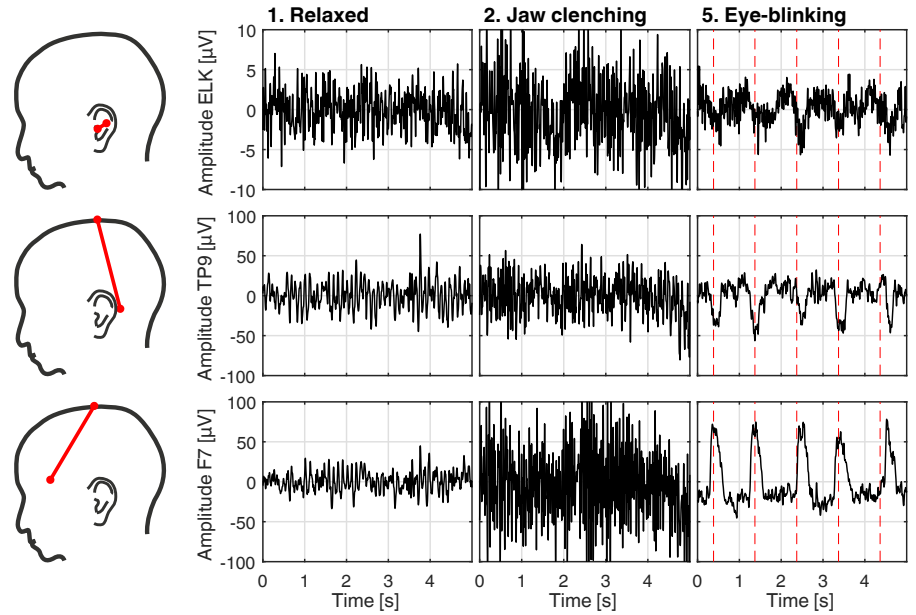

Figure 3.2: Time domain examples of artifacts recorded from a single subject. The first row shows recordings from the ELK ear electrode referenced to the ELB ear electrode. The second and third row are recordings from the TP9 and F7 scalp electrodes referenced to the Cz electrode. The sketches to the left illustrate the position of the reference and measuring electrode. The plots show raw EEG data band-pass filtered from 1 to 40 Hz. The red dashed lines for the eye-blinking condition indicate the eye-blink cue. [Figure and caption from [P1]]

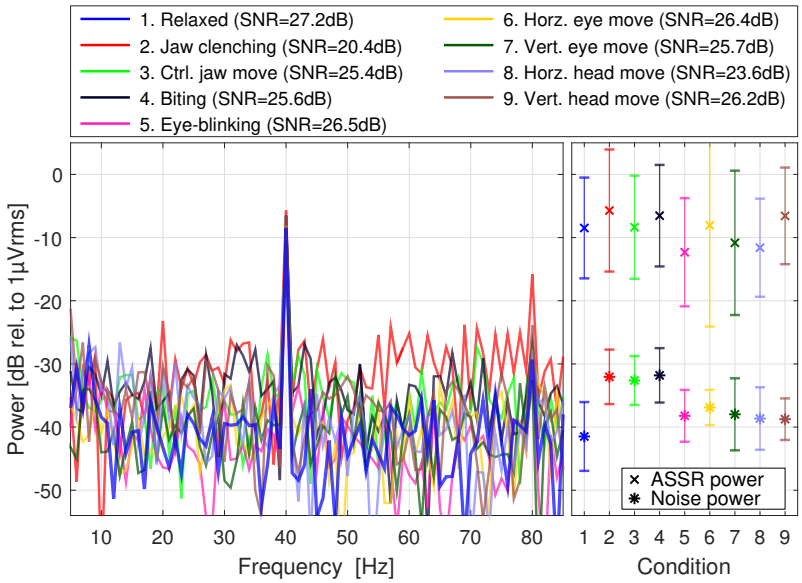

Figure 3.3: The plot to the left shows the grand average power spectra for the ELK left ear-canal electrode referenced to the ELB electrode. Grand average SNR values are given in the legend. The SNR values are based on the SNRD values for the frequency range 35 to 45 Hz given in Fig. 7 in paper P1. The power spectra are based on TDA of 64 segments of 1 s and a random overlap of 0.25 to 0.50 s. The markers on the right plot indicate the grand average ASSR power and mean noise power from 35 to 45 Hz, the error bars denote ±1 standard deviation. [Figure and caption from [P1]]

The left panel in Figure 3.3 shows grand average power spectra for the ELK electrode referenced to the ELB electrode, and the right panel display the mean and standard deviation of the ASSR power and the noise power from 35 to 45 Hz, for the 9 conditions.
Figure 3.3 shows the highest SNR deterioration (SNRD) for jaw clenching. This is consistent with previous studies of scalp EEG, which confirm major artifacts from jaw clenching [45]. The remaining artifacts only caused a minor SNRD, as it can be inferred from the SNR values in the legend.

Paper P1 presents SNRD values for 32 scalp and 8 ear electrode locations. The overall picture was that the SNRD values for the temporal lobe scalp electrodes and the ear electrodes were very similar. Artifacts related to eye-blinking were high in frontal region electrodes, and lower in both the ear electrodes and temporal lobe region scalp electrodes. Looking at both scalp and ear electrodes, the most deteriorating artifact was jaw clenching, which confirm the observations for Figure 3.3.

The quantitative study of artifacts, presented above, was based on the ASSR. In order to investigate the quality of spontaneous EEG recorded with ear-EEG, alpha band modulation (ABM) were studied in an open/closed eyes paradigm [P1]. The

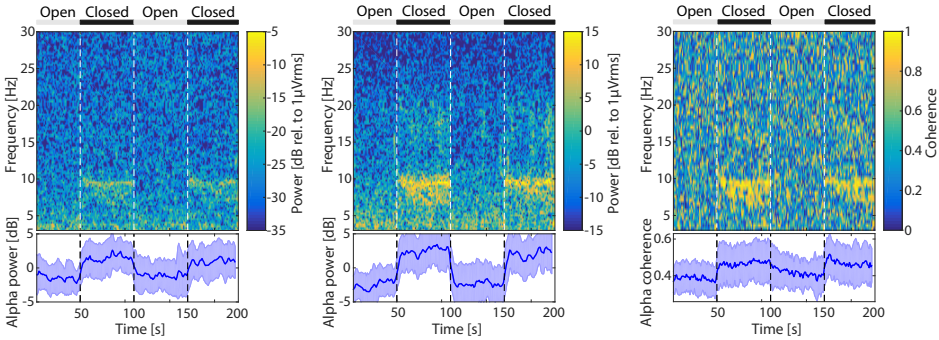

(a) Power spectrogram for ERE. (b) Power spectrogram for TP10. (c) Coherence spectrogram for ERE and TP10.

Figure 3.4: The top row show typical power and coherence spectrograms for one subject. The plots below the spectrograms are the grand average alpha power and coherence. (a) Power spectrogram of a right ear-EEG electrode, ERE, referenced to the ERB electrode (b) Power spectrogram of a scalp electrode behind the right ear, TP10, referenced to the Cz electrode (c) Spectrogram of the coherence between ERE and TP10. The white lines indicate changes between open and closed eyes. The faded areas of the grand average plots are the standard deviations of the grand averages. [Figure and caption from [P1]]

paradigm and data analysis are detailed in paper P1. Figure 3.4 shows typical power and coherence spectrograms for the ERE and TP10 electrodes for one subject, and grand average alpha power and coherence for 9 subjects below the spectrograms. The closed eyes intervals are clearly distinguished by increased alpha power and coherence, which corresponds well with ear-EEG results for a similar paradigm presented in paper P9. The increased alpha coherence for the closed-eyes intervals could indicate a common source of the alpha oscillations observed in electrode ERE and TP10.

The results from the lab study of artifacts and spontaneous EEG are promising for the development of ear-EEG based devices for monitoring of EEG in real-life settings.

3.2 Real-life study of artifacts

The lab study of physiological artifacts investigated real-life artifacts in a controlled laboratory environment. To accompany the lab recordings of physiological artifacts, a study of artifacts in 4 real-life settings were conducted for 3 subject and presented in paper P6. The real-life settings were:

1. **Walk outside**: Walk on the sidewalk of the city streets.
2. **Walk in mall**: Shopping and walk in a shopping mall.
3. **Relax in mall**: Relaxing on a bench in a shopping mall.
4. **Cycling**: Cycling up and down hill on a bicycle path.

Figure 3.5: Left: Pictures of the instrumentation used to perform recordings in real-life settings. Right: Pictures taken during recordings in the walk outside and cycling settings.

Figure 3.5 shows pictures of the instrumentation and two of the real-life settings. The experimental setup is detailed in paper P6.

Similar to the lab study of physiological artifacts, the recordings were performed while the subject was stimulated with an auditory steady-state stimulus. This enabled comparison of the SNR for a relax in the lab setting and the real-life settings. Thus, the SNRD could be calculated for each of the artifact settings. The study generally showed a higher SNRD for the scalp EEG recordings with a Cz reference compared to the ear-EEG recordings, where the reference was the ELB electrode for the left ear and the ERB electrode for the right ear. For both scalp and ear-EEG the lowest SNR values were observed for cycling, which correspond to expectations of a high level of muscle activity and motion needed for cycling.

EEG were also acquired while the subject were walking on the sidewalk with no applied stimulus. The analysis showed high coherence between ear and behind-the-ear electrodes for frequencies from 10 to 40 Hz. It is likely that the source of the high coherence was physiological, and could be electrical activity in muscles.

The study was an early attempt at performing real-life ear-EEG recordings, and confirmed expectations of a higher noise level in real-life [P6]. With the lab study of physiological artifacts in mind, it was clear that not all the measured real-life artifacts had a physiological origin. Some of the non-physiological artifacts were probably related to the EEG amplifiers[1] available for the study. The amplifiers did not utilize active shielding (guarding) of electrode cables, which caused the setup to be sensitive to cable motion and capacitively coupled noise. In addition, the current noise of the amplifiers were measured to be 2-3 times higher than the current noise of the g.USBamp (g.tec, Austria) amplifier, which has been used for previous studies of ear-EEG in the laboratory [P1, P5, 55].

[1]The study was performed with Avatar EEG amplifiers (EGI, USA).

Chapter 4

Dry-contact ear-EEG

A crucial aspect of wearable EEG is to achieve an acceptable level of user-friendliness and comfort while maintaining an adequate measurement quality. A significant improvement in the user-friendliness and comfort can be obtained by avoiding the use of electrode gel. Bio-potential surface electrodes which are not actively supplied an electrolyte are called dry-contact electrodes. Within the latest years dry-contact electrodes have been given a lot of attention in the research community, and various electrode designs have been proposed. This includes mesh electrodes laminated onto the skin [79], electrodes based on flexible polymers [57, 41, 58] and spring loaded electrodes [40, 24]. The research within dry-contact electrodes mainly focuses on two aspects; 1) design of the electronic instrumentation to handle dry-contact electrodes [94], and 2) design of the electrode to accommodate and reduce variations in the electrode-skin interface [23]. This chapter addresses both aspects: Section 4.1 describes a novel dry-contact electrode design for ear-EEG, Section 4.2 presents studies of the skin-electrode impedance for different ear-EEG electrodes, and Section 4.3 introduce a low power and custom made electronic instrumentation platform for acquisition of ear-EEG with dry-contact electrodes.

4.1 Ear-EEG electrodes

Previous ear-EEG recordings have been acquired with wet electrodes, where a conductive gel was applied between the skin and electrode to improve the electrode-skin interface [P1, P5, P9, 55, 62]. Paper P2 presents a study of a novel dry-contact electrode design for ear-EEG. The electrodes, described in the paper, were made of a titanium (Ti) pin coated with iridium-oxide (IrO_2). IrO_2 is a well-characterized coating with pseudocapacitive properties and low impedance, which makes it attractive for stimulation electrodes [74, 27]. The coating has also been used for pH electrodes [54], and studies have shown great properties of IrO_2 coated electrodes for measuring physiological potentials [35, 28]. The dry-contact electrodes studied in paper P2 were coasted with a thermal iridium oxide film (TIROF) formed on an

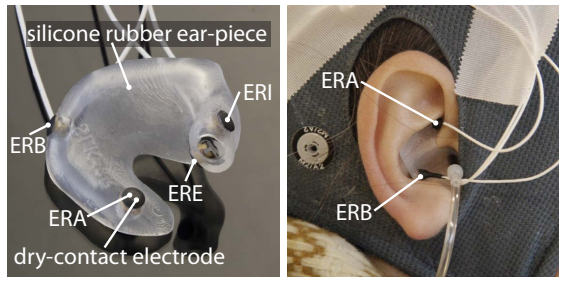

Figure 4.1: Left: Dry-contact electrodes inserted in a silicone rubber earpiece. Right: The earpiece inserted in the ear. [Figure modified from Fig. 1 in [P2]]

etched titanium pin [14, 72].

Mechanically, the electrodes were developed to be pushed through a hole in a soft silicone rubber earpiece as shown in Figure 4.1. Previous ear-EEG earpieces have been 3D printed in rigid acrylic plastic, and electrodes have been painted on the surface of the earpiece with silver epoxy. Thus, the electrodes could not be reused for another earpiece. The dry-contact electrodes presented in paper P2 were generic and could be inserted in individually designed soft earpieces, and moved from one earpiece to another.

The mechanical construction of the electrodes is illustrated in Figure 4.2. The IrO_2 coated Ti pin was inserted into a plastic housing plated with gold on the outside. The shield of a coax cable was connected to the gold plated housing to create a shielding body and the core of the same coax cable was connected to the Ti pin. Epoxy glue was applied in the housing to increase the mechanical strength of the construction and finally the electrodes was closed with a shielding lid.

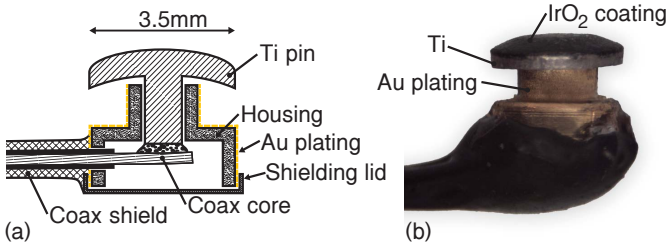

Figure 4.2: (a) Sketch of the dry-contact IrO_2 electrode design. (b) Microscope picture of the designed electrode. [Figure and caption from [P2]]

The soft earpieces mentioned above were made of soft silicone rubber and customized to the anatomical shape of the user's ear. The double-curved and concave surface of the ear facilitate the earpieces to stay in place, and the flexibility of the soft earpiece enable it to adapt to changes in the shape of the ear, caused by e.g. jaw movements. This helped the electrodes to maintain a stable and comfortable contact with the skin. However, from the practical experiences involved in performing

the recordings presented in paper P2, it is clear that further development of the flexible earpieces are needed, to obtain the goal of a stable contact with the skin in real-life situations. Challenges with stable impedances of the electrode-electrolyte interface (EEI) were especially observed for electrodes in the concha region of the ear [P2].

4.2 Electrode-skin impedance

A prerequisite for measuring EEG of high quality with a conventional EEG amplifier and wet electrodes, is to have a low and stable electrode-skin impedance. When moving to dry-contact ear-EEG electrodes, low and stable impedances are challenged by the absence of gel and the presence of hair and earwax.

Traditionally, the electrode-skin interface has been modelled as an electrochemical EEI. Low impedance of the EEI is important for mainly two reasons 1) The impedance generates thermal noise as described by the Johnson-Nyquist equation. 2) The amplifiers current noise is converted to voltage noise through the impedance. This means that everything else being equal, a higher impedance of the EEI will increase the noise level. EEG signals are measured as potential differences between two (or more) electrodes. Due to a finite input impedance of the instrumentation amplifier, an impedance mismatch between two electrodes will transform a common-mode signal on the body to a differential-mode signal on the input of the instrumentation amplifier. This causes the common-mode rejection ratio (CMRR) of the instrumentation to be limited by $CMRR_{elec}$, as described by equation 4.1 [94].

$$CMRR_{elec} \cong 20 \cdot \log_{10}\left(\frac{Z_C}{\Delta Z_E}\right) \tag{4.1}$$

where ΔZ_E is the impedance mismatch and Z_C is the common mode input impedance of the instrumentation amplifier.
The amplitudes of ear-EEG recordings are in the range of a few microvolts and common-mode noise on the body can be in the volts range [87]. Hence, to enable meaningful recordings of ear-EEG, the CMRR of the complete instrumentation must be at least 120 dB [P4]. In order to obtain a CMRR of 120 dB with an impedance mismatch of e.g. 1 MΩ, the input impedance of the instrumentation amplifier must be at least 1 TΩ, according to equation 4.1. Thus, trade-offs between CMRR and noise performance need to be considered in the design of an appropriate instrumentation amplifier [P4].

Paper P4 presents measurements of the EEI impedance for wet and dry-contact ear electrodes made of silver (Ag), and paper P2 describes similar measurements for ear electrodes coated with IrO_2. Figure 4.3 summarizes the measurements in model parameters, where the impedance of the EEI was modeled by a capacitor and resistor in parallel and in series with a resistor, as illustrated by the circuit drawing to the right in Figure 4.3. Comparing wet and dry-contact Ag electrodes,

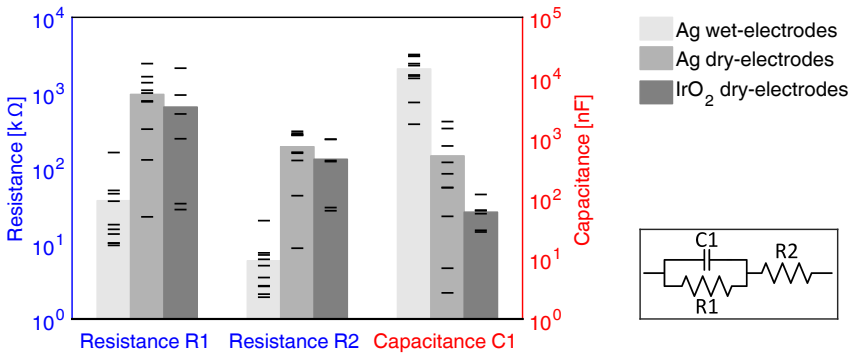

Figure 4.3: Grand averaged parameter values for different electrode materials. The impedance spectrum of the EEI was modeled by the parametric model shown to the right. The black lines indicate parameter values for single recordings [Figure from [P2]].

the mean and variance of R1 and R2 were one to two orders of magnitude higher for dry-contact electrodes, as illustrated in Figure 4.3 and detailed in paper P4. Additionally, the capacitance of the dry-contact electrodes were lower than the capacitance of the wet electrodes, which could be explained by differences in how the capacitance is formed, as described in paper P5. Comparable resistances and capacitance were observed for the dry Ag and dry IrO_2 electrodes, though the area of the IrO_2 electrodes were about 1.5 times smaller than the area of the dry Ag electrodes. Thus, for same size electrodes it seems reasonable to conclude that the impedance of the EEI would be lower for dry-contact IrO_2 electrodes compared to dry-contact silver electrodes.

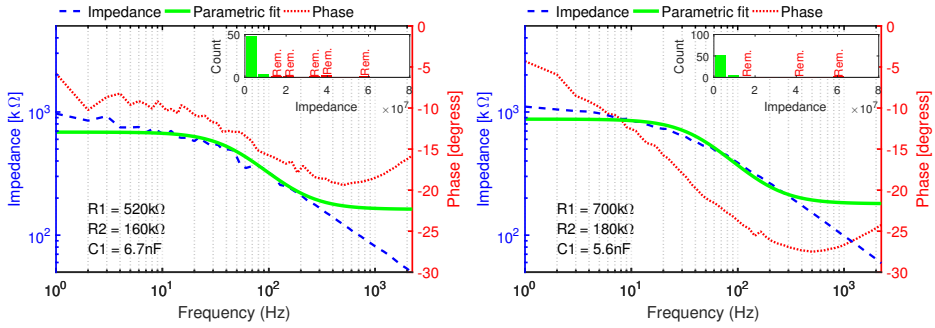

(a) Dry-contact IrO_2 electrodes in the ear-canal (b) Dry-contact IrO_2 electrodes in the concha

Figure 4.4: Impedance spectra for the IrO_2 dry-contact electrodes. All impedance measurements were performed with the ear-piece inserted in the ear of a subject. The histogram in the upper right corner show the distribution of the mean impedance from 0.1 Hz to 10 Hz. A few recordings, marked by "Rem.", were outliers in the histogram and left out of the analysis [Figure and caption from [P2]].

The impedance spectra in Figure 4.4 shows the grand average impedance for the dry IrO_2 ear electrodes located in the ear-canal and concha part of the ear. The figure display a similar impedance spectrum for the electrodes in the ear-canal and concha. The study of dry-contact Ag electrodes, presented in paper P4, did not include measurements from electrodes in the concha, because the skin contact was too unstable. Figure 4.4 shows that with soft earpieces and IrO_2 electrodes, acceptable impedances can be obtained, also for electrodes located in the concha. However, it should be mentioned that it was challenging to maintain a stable EEI impedance for the concha electrodes in real-life settings [P2].

4.3 Electronic instrumentation

The electronic instrumentation for acquisition of EEG signals can be divided in to two main components; the analog front-end and the analog-to-digital converter (ADC). The analog front-end amplifies the high impedance signal, measured on the body, to a low impedance signal that can be digitized by an ADC.

Here we will focus on the development of electronic instrumentation, enabling high quality ear-EEG recordings with the dry-contact IrO_2 electrodes presented in Section 4.1. Apart from enabling high quality recordings, the instrumentation was designed to allow implementation in a device with hearing aid form factor, which enable recordings of ear-EEG in real-life for at least 24 hours on a standard hearing aid battery. A hearing-aid-sized ear-EEG device would also include a microcontroller and memory for storage or a radio for transmission of the EEG data [62]. Thus, the power consumption of the instrumentation must be in the order of sub-mW, for such a device to be powered by a standard hearing aid battery[1] for at least 24 hours [22]. Because of small electrode distances in the ear, the amplitude of the ear-EEG signal is approximately 20 dB lower than the amplitude of conventional EEG. This demands an instrumentation amplifier with low noise [55]. As given in Section 4.2 the mean and variance of the EEI impedance are one to two orders of magnitude higher for dry-contact electrodes compared to wet electrodes [P4]. This requires a low bias current and current noise, to avoid saturation and to maintain a low noise level of the recordings. In addition, the higher variance of the EEI impedance for dry-contact electrodes indicates that impedance mismatch between electrodes can easily arise. An impedance mismatch in the order of 1 MΩ demands an input impedance in the TΩ range, in order to maintain sufficient CMRR, as described above and in paper P4.

To meet these requirements, a custom electronic instrumentation platform based on two application specific integrated circuits (ASICs) were developed by Zhou et al. and described in paper P7.The development of the ASICs was not a part of this project. However, the characterization of the dry-contact electrode

[1] Hearing aids are usually powered by zinc-air batteries. A commonly used battery is the size 10 (A10) battery, with a typical capacity of about 100 mAh.

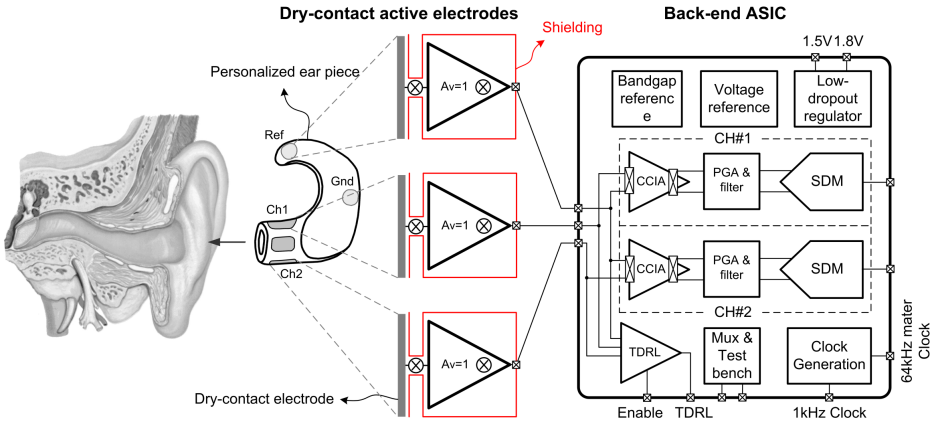

Figure 4.5: Blockdiagram of the custom electronic instrumentation platform designed for measuring ear-EEG with dry-contact electrodes in real-life settings. [Figure from [P7]]

interface, described in Section 4.2, provided fundamental input to the specification of the developed instrumentation. In addition, validation of the developed instrumentation through ear-EEG recordings was performed as a part of this project. The developed electronic instrumentation platform is illustrated in Figure 4.5 and comprise three identical ASICs implementing a unity buffer and an ASIC implementing a back-end (BE). The buffer ASICs were designed to buffer the signal close to the electrodes, creating an active electrode (AE). An additional function of the buffer was to drive the shield of the dry-contact electrode, creating an actively shielded (guarded) electrode. The active shielding reduces electrical interference and minimizes the parasitic capacitive load from the shield to the signal wire. The main components of the BE ASIC, were an instrumentation amplifier, transconductance driven-right-leg (TDRL), programable gain amplifier (PGA) and sigma-delta modulator (SDM). Chopper circuits were implemented on the input and output of the buffers and instrumentation amplifier to modulate and demodulate the signal. Chopping is a standard technique to remove amplifier DC offset and reduce 1/f noise generated by the amplifier. As illustrated in Figure 4.5 the instrumentation platform enables recordings from 2 electrodes with a common reference electrode. A fourth electrode is used for the TDRL or a passive GND. The BE ASIC outputs the raw delta/sigma bit streams from the SDMs. A standard 8-bit USB module[2] was used to interface with a computer, and the data were collected and decimated using Matlab R2016a (Mathworks Inc., Natick, MA, USA).

Figure 4.6 shows the measured performance of the instrumentation platform illustrated in Figure 4.5. Table 4.1 summarizes the measurements and compare the performance with state-of-the-art. With the chopper frequency set to 1 kHz the

[2]The USB interface were based on the UMFT240XE development module from Future Technology Devices International Ltd (FTDI).

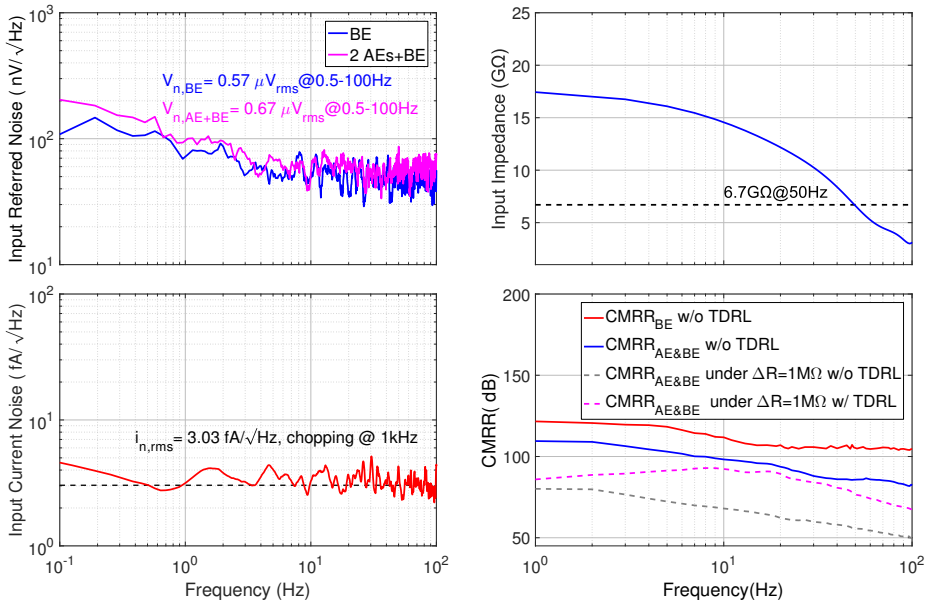

Figure 4.6: Measured performance of the electronic instrumentation developed by Zhou et al. [P7]. Top left: input referred noise. Top right: input impedance. Bottom left: current noise. Bottom right: CMRR. [Figure modified from [P7]]

Parameters		Xu et al., 2014 [102]	Guermandi et al, 2015 [46]	Ha et al., 2015 [47]	Xu et al., 2015 [101]	Zhou et al., 2016 [P7]
Supply [V]		1.8	3.3	1.2	1.8	1.8
Active electrode		✓	✓	✗	✓	✓
input referred noise (IRN) [V_{rms}]		1.75	0.28	1.2	0.65	0.67
Input impedance [GΩ]	@DC	~2	–	–	~1	~18
	@50Hz	~0.3	0.1	1@60Hz	~0.1	6.7
Current noise [fA/√Hz]		–	–	–	20@f_{chop}=4kHz	~3@f_{chop}=1kHz
Offset tolerance [mV]		±250	–	±200	±350	> ±200
CMRR [dB] @50Hz	w/o CMRR enhancement	~60	64	100	<60	86
	w/ CMRR enhancement	84 (CMFF)	–	132 (CMFB)	102 (CMFF)	108 (TDRL)
	w/ impedance mismatch	–	–	–	42/ΔZ_E=800kΩ	78/ΔZ_E=1MΩ
Current per channel [A]		46	120	7.4	58	60
Dry-contact application		✓	✗	✗	✓	✓

Table 4.1: The instrumentation developed by Zhou et al. [P7] compared with state-of-the-art.

total input referred noise (IRN) was measured to 0.67 Vrms in the frequency range 0.5-100 Hz. The input impedance is plotted top-right in Figure 4.6, and shows an input impedance close to 18 GΩ@DC and 6.7 GΩ@50Hz. This is more than 6 times higher than the input impedance reported by Ha et al. [47]. The bottom-left plot shows the input current noise, with an average of 3.0 fA/$\sqrt{\text{Hz}}$, which is about 6

times lower than state-of-the-art [101]. The CMRR is plotted bottom-right and displays a CMRR for the instrumentation platform (AE&BE) at about 110 dB@DC. With a 1 MΩ impedance mismatch between electrodes, ΔZ_E, the CMRR was measured to 56 dB@50Hz. When the TDRL was activated, the CMRR improved to 78 dB@50Hz. Thus, the desired CMRR of 120 dB has not been achieved, even thought the CMRR with TDRL activated is 36 dB higher than [101]. Mismatches of up to 1 MΩ could occur with the IrO_2 dry-contact electrodes, where the mean impedance of 44 electrodes mounted in earpieces was measured to Z_E@47Hz=510 kΩ with a standard deviation of σ_{Z_E}@47Hz=760 kΩ [P2]. This illustrates the challenges involved in obtaining sufficient CMRR for dry-contact electrodes.

4.3.1 Prototype platforms

As described above, the instrumentation ASICs were designed to be implemented in an ear-EEG device with hearing aid form factor. The first step towards this goal was the development of a flex PCB, which could be mounted in an earpiece as shown in Figure 4.7(a). The BE ASIC was mounted centrally on the PCB via a ceramic substrate and the AE ASICs were mounted on the backside of each electrode, also by utilizing a ceramic substrate. However, debugging was problematic with this design, and it was difficult to mount the flex PCB in an earpiece without damaging the PCB. In addition, the rigidity of the flex PCB often created unwanted deformation of the earpiece, and reduced the flexibility of the earpiece. These aspect contributed to a more unstable EEI and sometimes the earpiece caused unpleasant pressure in the ear. In order to decouple electrical and mechanical problems, and thereby make problem solving easier, the instrumentation ASICs were mounted in carriers on a conventional PCB. The PCB was build into an external box (matchbox) as shown in Figure 4.7(b). Electrodes were connected to the matchbox-system via high quality

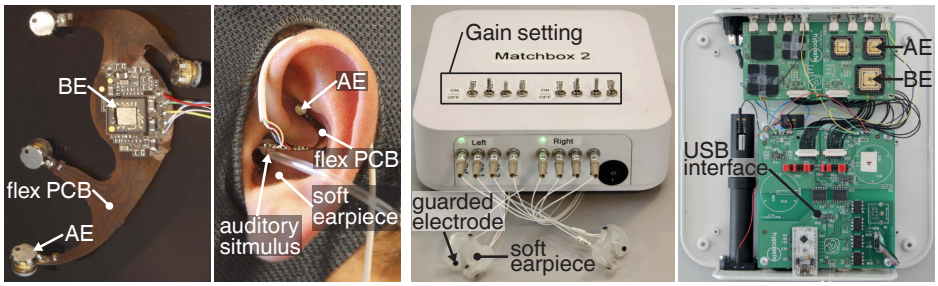

(a) ASICs mountes on flex PCB

(b) Instrumentation platform in external box.

Figure 4.7: (a) left: The instrumentation ASICs mounted on a flex PCB together with dry-contact IrO_2 electrodes. (a) right: Flex PCB mounted in an earpiece and inserted in to the ear of a subject. (b): The instrumentation ASICs mounted in carriers on a PCB in an external box (matchbox).

coax connectors, in order to extend the active shielding all the way from the buffer to the backside of the electrode. In addition, the connectors made it easy to change between different electrode configurations. For this design, the active shielding (guarding) of the cables and electrodes were crucial to obtain low noise ear-EEG recordings from the dry-contact electrodes.

4.3.2 Ear-EEG recordings

To test the matchbox-system, recordings were performed with the dry-contact IrO_2 electrodes inserted into a flexible earpiece, as detailed in paper P2. Measurements were acquired from one subject for an open/closed eyes paradigm and an ASSR paradigm. The experimental setup and stimulus for the paradigms were identical to the paradigms detailed in paper P2. Both recordings were performed with an ERI ear electrode, referenced to ERA, and with a passive GND (w/o TDRL) electrode located in the ERB position, as illustrated in Figure 4.5.
Figure 4.8 shows clear ABM related to open/closed eyes. The power in the alpha band (8-12 Hz) is increased for closed eyes intervals, which is consistent with ear-EEG recordings performed with wet electrodes [P1, P9].
Figure 4.9 shows the ASSR recorded during auditory stimulation with white noise

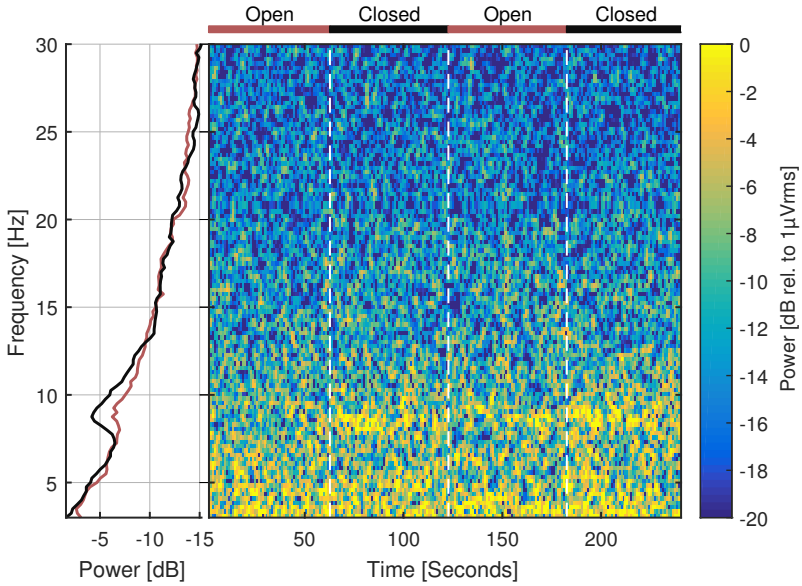

Figure 4.8: Power spectrum (left) and spectrogram (right) for an alpha-band modulation experiment for one subject. The recording was acquired with an ERI ear electrode referenced to ERA. The subject condition (open or closed eyes) is indicated above the spectrogram. The power spectrum is shown for the open-eyes condition (red line) and the closed-eyes condition (black line) respectively.

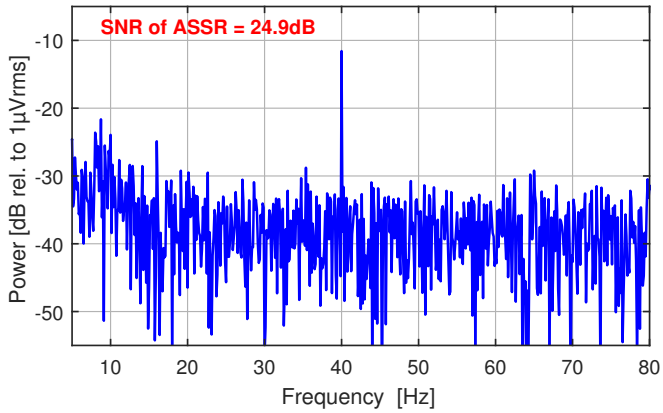

Figure 4.9: Power spectrum for an ASSR recording from an ERI ear electrode referenced to ERA.

amplitude modulated with 40 Hz. The SNR of the ASSR is comparable to previous ear-EEG recordings performed with wet electrodes [55, P9, P1].

These very initial results are promising for the application of the developed electronic instrumentation in ear-EEG devices with hearing aid form factor. However, further studies of ear-EEG, measured with the matchbox system and dry-contact electrodes, are needed to fully document the performance of the developed instrumentation.

Chapter 5

Real-life ear-EEG

Many years of research have focused on understanding the brain in restrained laboratory conditions, and much relevant research has been performed under these conditions. However, laboratory studies typically don't mimic real-life situations very well. Measurements of EEG in real-life situations could improve the understanding of spontaneous EEG related to everyday life situations, and open up new fields of applications and research within evoked potentials [24]. For evoked potentials, previous studies of mice have shown that visual and auditory evoked potentials are significantly different when the mice are moving as compared to not moving [77, 89]. It seems reasonable that similar results could apply to human studies; i.e. brain responses measured in real-life settings are different from responses measured under restrained laboratory conditions. Recordings of EEG in real-life should be performed without affecting the users everyday life [33]. Thus, EEG de-

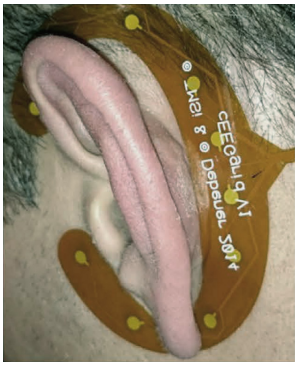

(a) The cEEGrid EEG device [Figure from [32]]

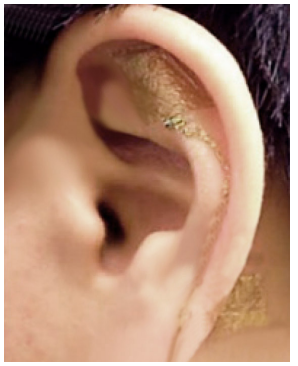

(b) Electrodes laminated onto the skin [Modified from [79]]

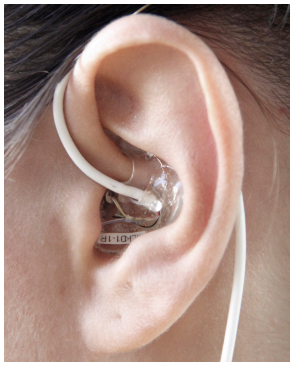

(c) Ear-EEG device [Figure from [P1]]

Figure 5.1: Examples of wearable EEG electrode systems based on measuring the EEG from electrodes around the ear (a), on the ear (b) or in the ear (c).

vices for real-life brain-monitoring must be wearable, discreet, user-friendly, and unobtrusive to everyday life activities and enable long-term monitoring of EEG [22]. Most commercial wearable systems are based on standard scalp montages, which typically cause the systems to be clearly visible and in most cases uncomfortable to wear for long-term recordings. Some research projects focus on designs for long-term monitoring, which do not attract attention during everyday life activities. Figure 5.1 shows three examples, where the EEG is measured around the ear (5.1(a)), on the ear (5.1(b)) and in the ear (5.1(c)).

This chapter presents a real-life study of ear-EEG in Section 5.1. Section 5.2 covers a method for optimization of electrode configurations for ear-EEG, and Section 5.3 concerns ear-EEG used for BCIs.

5.1 Ear-EEG recordings

One of the main advantages of the ear-EEG method is the compact and discreet nature of ear-EEG devices, which support the vision of performing EEG recordings in real-life. However, to bring ear-EEG into everyday life, the device must be comfortable to wear and user-friendly. In order to address these aspects, dry-contact IrO_2 electrodes and a flexible earpieces were developed and described in Section 4 and paper P2.

Paper P2 also presents a study of real-life ear-EEG recorded with the dry-contact IrO_2 electrodes mounted in flexible earpieces. The recordings were acquired with a commercial EEG amplifier[1], which was characterized by a high input impedance ($>10\,G\Omega$), low noise ($<0.4\ \ V_{rms}$ @ 0.1...10 Hz) and actively shielded (guarded) wires. The study comprised four paradigms; auditory steady-state response (ASSR), steady-state visual evoked potential (SSVEP), auditory onset response (AOR) and alpha band modulation (ABM). The recordings were performed with the following stimuli:

ASSR Gaussian distributed white noise amplitude modulated with a 40 Hz sinusoid.

SSVEP Modulation of the ambient light with 9 Hz, performed with modified 3D shutter glasses [P2].

AOR 1 kHz sinusoid of duration 200 ms, with an attack and release time of 10 ms. The SOA was randomly selected between 1.7 and 2.3 s.

ABM An auditory cue indicated a change between open and closed eyes every 60 second.

The recordings of ASSR, SSVEP, and AOR had a duration of 5 minutes, and the ABM recordings had a duration of 4 minutes. The paradigms were recorded for 6 subjects in a lab setting, where the subjects were comfortably seated, and in a real-life setting, where the subjects were walking on the sidewalk of streets

[1]The EEG recordings were acquired by a 32 channel portable TMSi MOBITA EEG amplifier (TMSi, The Nederlands).

close to Aarhus University, Denmark. The recordings were analyzed with different reference configurations, as detailed in paper P2. Grand average results from the study are presented in Figure 5.2, 5.3 and 5.4 for a Cz reference configuration.

Figure 5.2(a) and 5.2(b) show a similar SNR of the ASSR for lab and real-life recordings for both scalp and ear-EEG electrodes, even though the noise level of the real-life recordings are consistently higher. The SSVEP recordings, presented in Figure 5.2(c) and 5.2(d), had a lower SNR in real-life, compared to the lab recordings. However, the power of the SSVEP was similar for the two settings, but because of an increased noise level in real-life the SNR was lower in this setting.

The AOR, presented in Figure 5.3(a) for both scalp and ear-EEG, clearly show the well know P_1-N_1-P_2 waveform, with comparable timing to previous ear-EEG recordings [55]. The real-life AOR shown in Figure 5.3(b) have a less distinctive waveform, but the overall course of the waveform is still recognizable.

The lab recordings of the ABM, presented in Figure 5.4(a), display a significant increase in the grand averaged alpha band power for closed eyes intervals. The same trend is present on the spectrogram for a single subject. In real-life the ABM was less prominent, though an increased alpha band power is observable on both the spectrogram and the plot of the grand average alpha band power.

Generally, the recordings presented in Figures 5.2, 5.3, and 5.4 show comparable

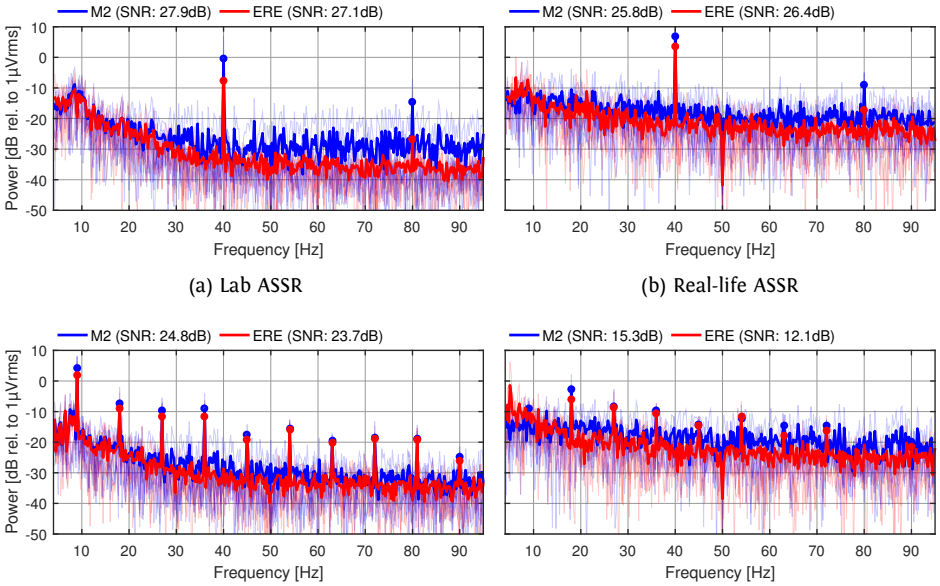

(a) Lab ASSR (b) Real-life ASSR

(c) Lab SSVEP (d) Real-life SSVEP

Figure 5.2: Grand average power spectra of the ASSR (top row) and SSVEP (bottom row) for a Cz reference configuration. The faded lines are the response for each subject. The grand average SNR are given for M2 and ERE in the legend of the power spectra. [Figure and caption from [P2]]

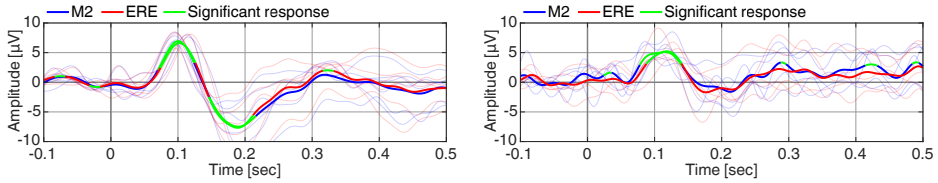

(a) Lab AOR (b) Real-life AOR

Figure 5.3: Grand averaged onset responses for a Cz reference configuration. The faded lines are the onset response for each subject. The green line intervals indicate a grand averaged response significantly ($p<0.05$) different from zero, measured by a one sample t-test. [Figure and caption from [P2]]

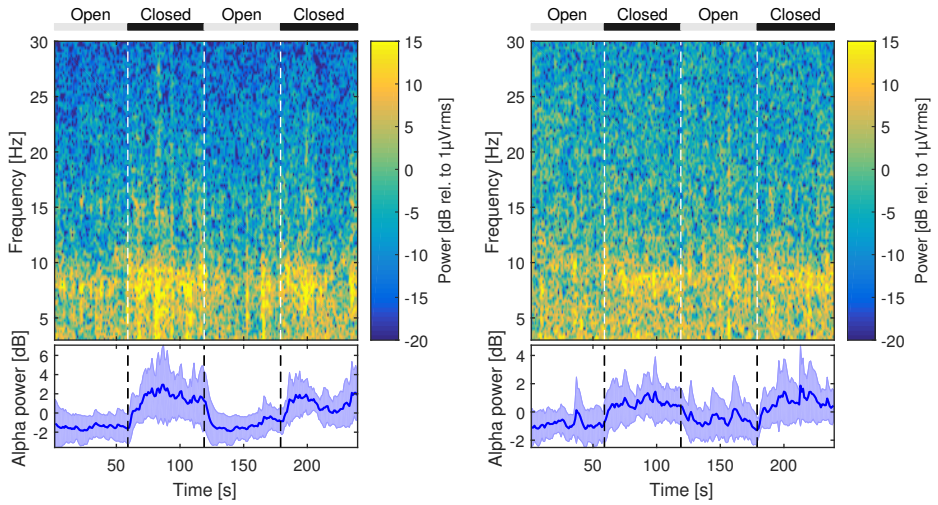

(a) Lab ABM (b) Real-life ABM

Figure 5.4: Spectrograms for one subject with indication of open and closed eyes intervals, recorded with ERE ear electrodes referenced to Cz. The plots below the spectrograms show the grand average of the mean power in the alpha band (8-12 Hz). The grand average plots have been smoothed with a 3 tap mean filter. [Figure and caption from [P2]]

performance of the ear and scalp electrodes when referenced to the Cz electrode. In addition, the figures display similar responses for the lab and real-life settings, albeit with significantly higher noise for the real-life setting. These results are promising for future applications of the ear-EEG platform in real-life.

Paper P2 also presents results for other reference configurations, which indicated increased challenges with noise in real-life, when the reference electrode was located in or close to the ear. The recording quality for electrodes located in concha were especially low in real-life, and indicate particular challenges with electrodes in this region of the ear. The main problem with noise and recording quality were

likely related to maintaining a stable impedance of the EEI, as described in Section 4.1. It is expected that further development of the earpieces and dry-contact electrodes can improve the stability of the EEI and increase the quality of real-life ear-EEG recorded with dry-contact electrodes.

5.2 Electrode configurations

The ear-EEG could be implemented in hearing aids, where an objective measure of the users hearing threshold would enable algorithms in the hearing aid to adapt to changes in hearing. The hearing threshold can be objectively estimated through measurements of the auditory steady-state response (ASSR) [61, 84]. The users of hearing aids typically wear them all day, which means that threshold estimation must work in real-life situations.

Studies of ASSR recorded with ear-EEG show variations in the power of the ASSR from subject to subject [55, P9]. Moreover, the optimal electrode configuration is not the same across subjects, and often changes between recordings from the same subject as well [P3]. It is reasonable to assume that inter-subject variations are related to differences in the neural responses and anatomy, intra-subject variations are more likely related to changes in the electrode-skin interface, which is typically more varying for real-life recordings [P2]. Methods are needed to handle these changes, to enable or increase the efficiency of hearing threshold estimation [17].

Paper P3 describes a method for optimizing a weighted average of electrodes, to obtain a high and robust SNR of an SSR. Optimization of the weights were based on the Fourier transform and the SNR of the first harmonic SSR.
To illustrate the method, consider an EEG signal recorded by L electrodes under steady-state stimulation. Initially, the EEG signal is re-referenced, TDA is performed to reduce noise of the SSR and the following are defined, as detailed in paper P3.

ω_{SSR}	modulation frequency of the stimulus.
$\bar{x}_l(m)$	TDA of the EEG data from electrode l, having M, $m=0,...,M-1$, samples.
$\bar{X}_l(\omega_{SSR})$	Fourier transform of $\bar{x}_l(m)$ at ω_{SSR}.
SNR_l	SNR of the first harmonic SSR.

Then, the SNR-Fourier vector, a_l, with a length of SNR_l and an angle of $\bar{X}_l(\omega_{SSR})$ is defined, as illustrated for 4 electrodes in Figure 5.5(a). The principal axes of the vectors are calculated, with the angle Θ to the principal axis of maximal variance. The SNR-Fourier vectors are rotated with the angle Θ, as shown in Figure 5.5(b). The $\mathbf{b}$ vector is then defined as the rotated SNR-Fourier vectors projection to the x-axis. Finally, the weight vector, $\mathbf{w}$, is calculated from $\mathbf{b}$, with zero mean and a total weight of the positive and negative contributions of 1 and -1 respectively

$$\mathbf{b} = \text{real}(\mathbf{a} \cdot e^{-i\cdot\theta}) \tag{5.1}$$

$$\mathbf{c} = \mathbf{b} - \frac{1}{L}\sum_{l=0}^{L-1} b_l \tag{5.2}$$

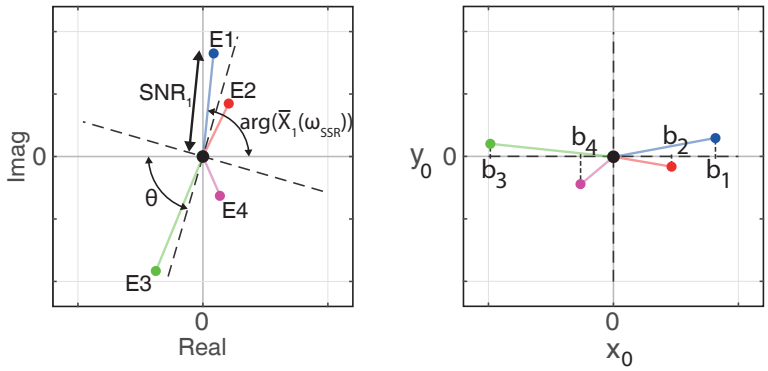

(a) (b)

Figure 5.5: (a) Plot of the SNR-Fourier vectors for 4 electrodes, with the principal axis of the vectors illustrated by the dashed lines. (b) The SNR-Fourier vectors rotated with the angle Θ, so the direction of maximal variance is parallel to the x-axis.

$$\mathbf{w} = \frac{2 \cdot \mathbf{c}}{\sum_{l=0}^{L-1} |c_l|} \quad . \tag{5.3}$$

The optimized reference configuration (ORC) is calculated by applying the weights to the EEG data

$$ORC(m) = \sum_{l=0}^{L-1} \bar{x}_l(m) \cdot w_l \quad . \tag{5.4}$$

ASSR recordings from 12 subjects were used to validate the method. Each of the recordings were divided in to a training and a test dataset. Figure 5.6 shows plots of the SNR-Fourier vectors for the training data from the 12 subjects. The plots clearly show that the weights must be trained for each subject individually, as there are large inter-subject variations in the optimal weighting of the electrodes.

The performance of the ORC is compared to other reference configurations in Figure 5.7. The "ELA ref." reference configuration was trained by fixing the reference to the ELA electrode, and then choose the electrode with the highest SNR for the training data. Similarly, training of the "SNR matrix" reference configuration was performed on the training data, where the combination of two electrodes with the highest SNR was selected. Figure 5.7 generally shows a higher SNR for the ORC compared to the other methods. This is confirmed by the grand average SNR given in the legend of the figure. The robustness of the ORC method to changes in electrode performance can be illustrated by subject 1, where the ORC give the lowest SNR for the training data. For the test data the SNR for "ELA ref." and "SNR matrix" reference configurations have decreased, which is likely due to changes in the electrode-skin interface. The ORC is robust to these changes, and outperforms the other reference configurations in this case.

When ear-EEG recordings are performed in real-life, new challenges must be addressed, and methods like this could prove to be an important step in the development of everyday life brain-monitoring.

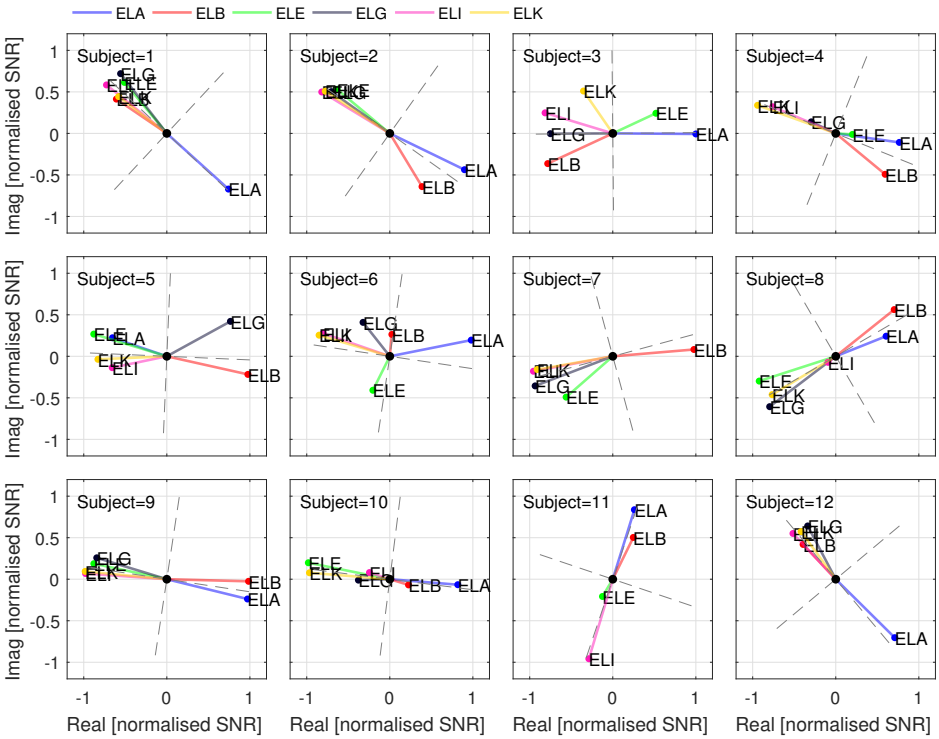

Figure 5.6: Plots of the SNR-Fourier vectors for the training data for recordings from 12 subjects.

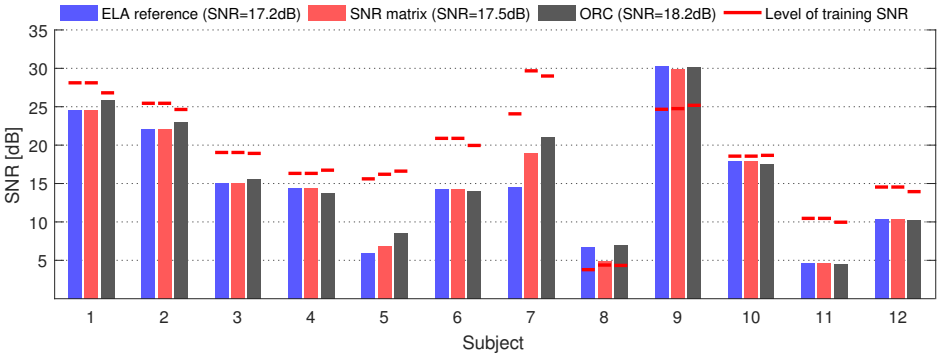

Figure 5.7: Bar plot of the SNR values calculated for the test data from all subjects and different reference configurations. The red lines indicate the SNR values for the training data. The mean SNR values for the test data are given in the legend.

5.3 Brain computer interface

A brain computer interface (BCI) enables a user to interface with a computer through monitoring of the user's brain responses. BCIs can be divided in three categories; active, reactive, and passive [105, 104].

- Active BCI: Intended alterations in brain response consciously controlled by the user and independent of external events. A typical example is motor imagery based BCIs.
- Reactive BCI: Unintended alterations in brain response, caused by a voluntary focus on an external stimuli. This includes P300 spellers and SSVEP based BCI.
- Passive BCI: Unintended alterations in brain response, automatically induced during interaction with the surroundings [105]. This includes machine interaction based on the users mental state [104].

BCI within all three categories could be relevant for ear-EEG, and would support various applications within e.g. hearings aids. The detection of SH, as described in Section 1.2, is an example of a passive BCI, where unintended alterations in the brain response related to SH triggers an alarm to the user about an impending SH.

Previous studies have demonstrated the relevance of reactive BCI for subjects with communication disabilities suffering from amyotrophic lateral sclerosis (ALS) or other severe damages to the central nervous system [50]. However, in order for reactive BCI to become a practical technology for this group of users, the robustness, comfort, required setup/cleanup time, and the amount of expert supervision must be reduced, when compared to conventional cap based systems [78]. Ear-EEG and dry-contact electrode technology addresses all of these aspects, and could be the enabling technology for a wider use of reactive BCI. Previous ear-EEG studies of a visual P300 based reactive BCI showed promising results, in terms of an average ITR of 17.4 bits/min (std=0.2 bits/min) reported by Farooq et al. [37] and an ITR of 8.3 bits/min reported by Bleichner et al. [18]. Paper P8 presents a SSVEP based reactive BCI system with similar performance, as described in the following.

Wang et al. developed a SSVEP based BCI system running on a mobile device for real-life BCI applications [99], and demonstrated a comparable performance for a similar system based on behind-the-ear electrodes [98]. Paper P8 presents a study of a corresponding SSVEP based BCI system utilizing ear-EEG. The ear-EEG was recorded from 12 ear electrodes (6 in each ear), referenced to an electrode located at the forehead. The SSVEP stimuli were presented on a 27-inch monitor displaying the layout in Figure 5.8. The subjects were asked to focus on one of the four squares, flickering between white and black. The detection algorithm was trained for each subject through 20 sessions. Each of the sessions had 12 trials and a duration of 60 s. Each trial contained 4 s for target gazing and 1 s for gaze shifting. The four stimuli were gazed three times in each session, in a random order.

An extended canonical correlation analysis (CCA) classification algorithm was trained as explained in [98] and an online experiment was performed. The online experiment showed an accuracy of 87.9 % (std=12.1 %), which is comparable to previous experiments with behind-the-ear electrodes [98]. The ITR was at 16.6 bits/min (std=6.6 bits/min), which is about half of what was previously obtained by Wang et al. [99, 98]. However, the stimulus layout for the study presented in paper P8 only utilized 4 targets, which naturally decrease the ITR compared to 12 targets in the previous studies by Wang et al. [99, 98]. The results are promising for future BCI applications of ear-EEG.

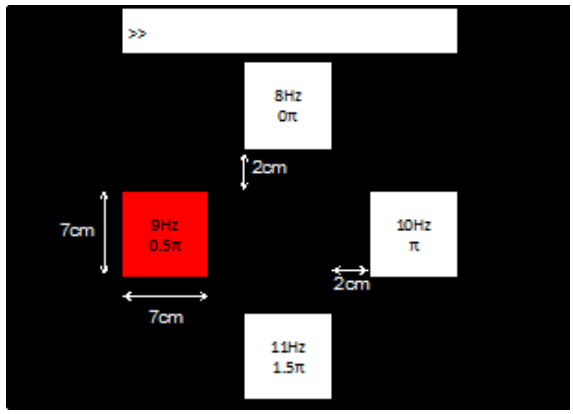

Figure 5.8: Visual stimulus layout for the SSVEP based BCI system presented in paper P8. The blank space in the top was used to show subject input. Each target was flickered with the frequency and phase indicated in the squares. For the training sessions, the color of the square were changed to red for 1 s to assist the subject to gaze on it. For the online experiment, the color of the square were changed to red for 1 s to indicate the decision by the system. [Figure from [P8]]

Chapter 6

Electric fields in the ear

This chapter describes a method for computing the electric fields on the scalp and the surface of the outer ear, from sources in the brain. The result of the method is a computational model, which describes the mapping of the electric fields from cortical sources to the scalp and ear. The value of such a model is illustrated in the following by means of a simple example.

Assume that the brain response to a specific stimulus at a specific point in time can be described by a finite number of dipoles in the brain. Propagation of the electric field from the dipoles to a point on the scalp (or in the ear) can be described by a linear function, and the potential in the point will be a superposition of contributions from the source dipoles. The surface of the outer ear is a complicated double-curved and concave surface, but for simplicity we can think of the potential field on this surface as a potential field in a plane. A simple example of this is illustrated as contour-plots in Figure 6.1.

Assume that 5 electrodes are distributed on the surface, with none of the electrodes

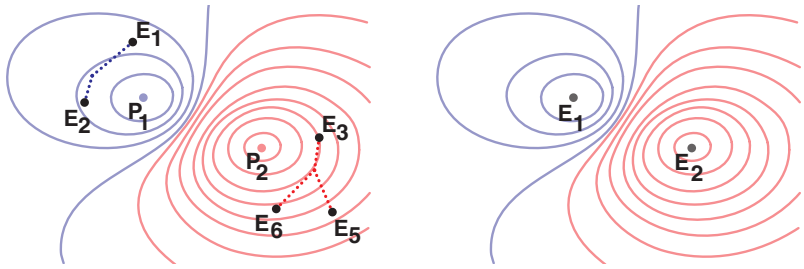

Figure 6.1: Sketch of contour plots of the potential on a surface. The black dots, marked with E_1 to E_6, are electrodes on the surface. P_1 and P_2 are locations of extreme potentials on the surface. (a) 5 electrodes distributed on the surface, with none of the electrodes located exactly at the extreme potentials. The dotted lines illustrate a weighted average of electrode signals (b) 2 electrodes placed at positions of extreme potentials.

located exactly at the extreme potentials, as illustrated in Figure 6.1(a). The highest potential difference on the surface will be measured between P_1 and P_2. Estimation of the potential at P_1 and P_2 is a trade-off between the number of measurement points and the available prior knowledge. With only a few electrodes and no prior knowledge available, the potential at P_1 and P_2 cannot be estimated, and the highest available potential difference will be between the two electrodes located at the highest and lowest potential, respectively.
If we instead assume that the contour plot was estimated by a computational model before locating the electrodes, then the electrodes could be located on top of the extreme potentials, as illustrated in Figure 6.1(b). This would increase the measured potential, compared to the example in Figure 6.1(a).
A model describing the propagation of the electric fields, from dipoles in the brain to the scalp (or the ear), is often refereed to as a forward model. The example above demonstrate how a forward model could provide valuable information on where to locate the electrodes on the earpiece, for a specific source distribution [18]. In addition, the model could increase the understanding of which responses that can be measured in the ear.

When recordings are performed in real-life, the noise level of recordings from the electrodes will be changing over time [P3]. With more than 2 electrodes available, the robustness to changes in electrode performance can be improved by calculating a weighted average of the signals from the electrodes, as detailed in paper P3 and illustrated by the dotted lines in Figure 6.1(a).

For the development of a forward model, it must be considered that the electrical field in the brain is attenuated by the skull, skin, cerebrospinal fluid (CSF) and the brain itself. Each tissue type have different electrical properties, and boundaries between the tissue types are very subject dependent [48]. Thus, in order to precisely model the electric field, individualized head models must be created [10]. The ears are usually very poorly described by head models, created by standard tools. This chapter presents a method for including the ears in head models. Section 6.1 introduce the procedures and tools for creating an ear-EEG forward model. Section 6.2 presents an example, where an ear-EEG forward model was used to map cortical sources to the ear.

6.1 Ear-EEG forward model

The most precise forward model is obtained by constructing a head model from anatomical scans of the subject [10]. T1 weighted magnetic resonance imaging (MRI) scans are the most commonly used modality. However, a combination of a computed tomography (CT) and a MRI scan would be preferable to obtain a precise description of both soft tissue and bone [12]. However, for research purposes it is typically not acceptable to perform CT scans, because of the X-ray radiation associated with a CT scan.

(a) (b) (c)

Figure 6.2: (a) Locations marked on an earpiece with Netfabb (b) The wax impressions oriented at a distance of 20 mm from the scalp mesh. (c) The wax impressions subtracted from the scalp mesh. [Click on the 3D objects (b) or (c) to zoom and rotate - only supported by Adobe Acrobat Reader.]

The neuroelectromagnetic forward-modeling toolbox (NFT), developed by Zeynep Acar el al. [11], is one of the available tools for generation of anatomically precise head models. The NFT supports whole head T1 weighted MRI scans performed with a voxel size of 1x1x1 mm. The toolbox includes tools for segmenting the MRI scan in brain, inner skull, outer skull and scalp meshes as described by Acar et al. in [11]. The relatively small size of the ears means that the anatomy of the ears cannot be precisely extracted from a whole head MRI scan. In order to obtain a precise model of the ears we propose a novel method, where 3D scanned wax impressions of the ears are used to model the ears. The 3D scanned wax impressions were aligned with the scalp mesh and subtracted from the head model, created using NFT. The procedure was:

1. Mark minimum 4 locations on each ear-EEG earpiece in the 3D viewer software Netfabb (Autodesk, CA, USA), as shown in Figure 6.2(a).
2. Digitize points (e.g. sensors/electrodes) on the scalp and the locations marked on the ear-EEG earpieces in the same coordinate system.
3. Align the coordinate system, of the digitized points on the scalp, with the scalp mesh, as described in [11].
4. Rotate and translate the 3D scanned wax impressions to minimize the least squared distance between the locations marked in Netfabb and the digitized locations.
5. Subtract the 3D scan of the wax impressions from the scalp mesh, as shown in Figure 6.2(b/c). To avoid intersections between the meshes, the distance between the meshes must be forced to a minimum of 1 mm.

Figure 6.3 shows the scalp, outer skull, inner skull and brain meshes for one subject. The meshes defines boundaries between the main tissue types in the head. Based on the assumption that the tissue between the boundaries are isotropic and ho-

mogeneous, the boundary element method (BEM) can be used to solve the partial differential equations associated with calculating the potentials on the scalp and in the ears [96, 12]. In order to reduce the complexity of the calculations, the potential is only calculated for predefined sensor locations. Similarly, a source space is defined, to reduce the number of possible source locations. For NFT, the sources in the source space, are only located within the brain mesh in a Cartesian 3D grid with a default grid size of 8 mm.

The potential at the sensor locations are related to the sources through the forward transmission coefficients defined in the lead field matrix (LFM), $\mathbf{A}$

$$\psi = \mathbf{A}\mathbf{x} \tag{6.1}$$

where, $\mathbf{x}$ is the vector of source currents, and the vector ψ is the potential at the sensor locations. Thus, each column of $\mathbf{A}$ describes the potentials at the sensor locations for a dipole in the sources space with unit amplitude. For each source location, 3 dipoles are defined in the LFM, with orientations parallel to the x, y or z-axis. Hence, $\mathbf{A}$ is a LxK matrix, where L is the number of sensors and K is the number dipoles, which is equivalent to the number of locations in the source space multiplied by 3, i.e.

$$\mathbf{A} = \begin{bmatrix} a_{11} & a_{12} & \cdots & a_{1K} \\ a_{21} & a_{22} & \cdots & a_{2K} \\ \vdots & \vdots & \ddots & \vdots \\ a_{L1} & a_{L2} & \cdots & a_{LK} \end{bmatrix} \tag{6.2}$$

where a_{lk} is the forward transmission coefficient describing the mapping from dipole k to sensor l. The potentials measured at the sensor locations can be approximated by a superposition of the dipoles described in $\mathbf{A}$ [88].

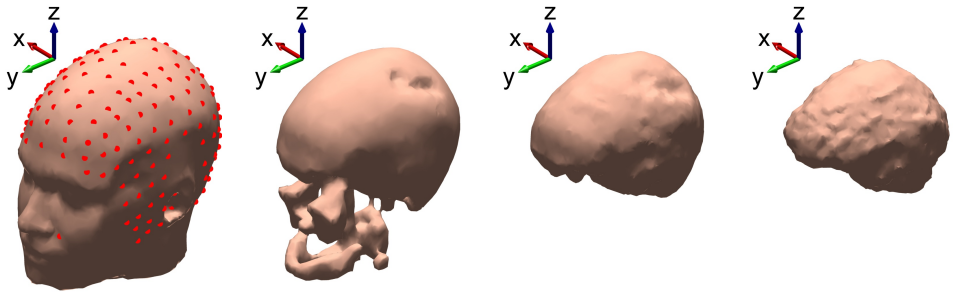

(a) Scalp (b) Outer skull (c) Inner skull (d) Brain

Figure 6.3: Mesh grids based on segmentation of a T1 weighted MRI scan, but where the ears are modelled by subtracting 3D scanned wax impressions of the ears from the meshes. The red dots on the scalp mesh indicate sensor locations. [Click on the 3D objects to zoom and rotate - only supported by Adobe Acrobat Reader.]

6.2 Mapping cortical sources to the ear

To illustrate the method described in the previous section, a head model was created for one subject. The head model was based on a whole head T1 weighted MRI scan and wax impressions of the subject's ears. Figure 6.3 shows the mesh grids for the head model. Based on the mesh grids, a forward model was calculated with the NFT toolbox. 205 sensors were evenly distributed on the scalp with a distance of approximately 20 mm, as shown in Figure 6.3(a). 6 sensors were located in each ear on the ExA, ExB, ExE, ExG, ExI and ExK locations, as described in Section 2.5. The source space had a grid size of 8 mm and the conductivities of the tissues were defined to: σ_{scalp}=0.33 S/m, σ_{skull}=0.0132 S/m, σ_{CSF}=1.79 S/m and σ_{brain}=0.33 S/m. The isolated problem approach (IPA) described by Acar et al. was activated for the BEM calculations [11]. The forward model is at present preliminary work and has not yet been validated with EEG data.

In Figure 6.4 on page 47 are shown potential maps for the x, y and z-orientations of a dipole located approximately in the right primary auditory cortex, and in Figure 6.5 on page 48 are shown potential maps for the x, y and z-orientations of a dipole located approximately in the right primary visual cortex. The first column in the figures shows plots for a dipole directed right lateral (x), the second column plots for a dipole directed frontal (y), and the third column plots for a dipole oriented dorsally (z). The first row in the figures shows the location and orientation of the dipole projected onto an MRI scan of the subject, the second row shows the potentials on the scalp with the color scale given below the plot, and the third and forth row contain plots of the potentials in the left and right ear, respectively, both with the color scale below the right ear. Each dipole was a normalized (1A) current dipole formed by two charges separated by 1 mm. The dipoles were located according to the Talairach coordinates[1] of the right primary auditory and visual cortices.

Electrodes located in a small area on the scalp will all be located in approximately the same plane. A consequence of this is that dipole sources oriented perpendicular to the plane, spanned by the electrodes, will be difficult to measure. The anatomy of the ear supports positioning of electrodes to span a 3D space, which enables measurements from dipoles with arbitrary orientation. However, the size of the ear limits the distance between electrodes. For comparison, the electrodes on the cEEGrid, developed by Debener et al. [32], are located around the ear in approximately the same plane, but with larger electrode distances, compared to ear-EEG. For some paradigms it could be necessary to locate electrodes both in and around the ear to span a 3D space, and also obtain larger electrode distances to

[1]The head model coordinates were co-registered with the generic Montreal Neurological institute (MNI) head model (available from www.bic.mni.mcgill.ca/software). The MNI coordinates for the specified cortices were then calculated by the Talairach to MNI coordinate converter tool provided by Yale University (available from sprout022.sprout.yale.edu/mni2tal/mni2tal.html). The tool provided by Yale University is based on the method described by Lacadie et al. [56].

increase the amplitude of the measured ear-EEG [19].
Figure 6.4 and 6.5 generally show big differences in the potential maps for the ears, for the different orientations and locations of dipoles. This emphasizes the need to distribute electrodes all over the surface of the earpiece to span a 3D space and thereby enable measurements of various dipole orientations and locations.

Figure 6.4 confirms previous ear-EEG studies of cortical auditory paradigms, like the ASSR, where the amplitude of ear-EEG were approximately 20 dB lower than the amplitude of behind-the-ear scalp EEG [55]. For visual sources, which are further away from the ear, the amplitude differences between ear-EEG and scalp were higher, as illustrated in Figure 6.5. This corresponds well to observations in previous studies, where the SNR of ear-EEG recordings from auditory paradigms have been higher than the SNR of recordings from visual paradigms [62, P9, P2].

The figures also show that slight changes in the orientation of a dipole can change the potentials in the ear significantly. For the same paradigm, slight changes in dipole orientation could be caused by differences in the anatomy of the brain between subjects. This could be one of the reasons for the inter-subject variations in the ASSR observed in paper P3.

Bleichner et al. emphasized the need for models to investigate the sensitivity of the ear-EEG to different brain processes, and requested a method to digitize the locations of ear electrodes [18]. The developed method addresses both of these aspects and has the potential to provide important information on the optimal electrode locations for measuring different brain processes.

6.3 Validation of the forward model

One way to validate a forward model is to compare EEG potentials measured by scalp and ear electrodes with potentials predicted by the forward model, for a similar source composition. The source composition is described by the source current vector, which could be estimated by a distributed source model for the measured EEG data or by utilizing a source decomposition method like ICA [88]. The paradigms for the recordings acquired during the visit at Swartz Center for Computational Neuroscience span from simple paradigms, like ASSR and SEP, to more advanced paradigms, including movie watching and game playing. The advanced paradigms were designed to activate multiple functional areas in the brain, and thereby enable validation of the model for sources distributed all over the brain. Recordings were acquired from 4 subjects by 12 ear, 205 scalp, 4 mastoid and 2 EOG electrodes, all digitized in the same coordinate system. In addition, T1 weighted MRI scans were performed for the subjects. The data enable high precision source localization by utilizing individual forward models. The recordings will be used to refine and validate the method described in Section 6.1.

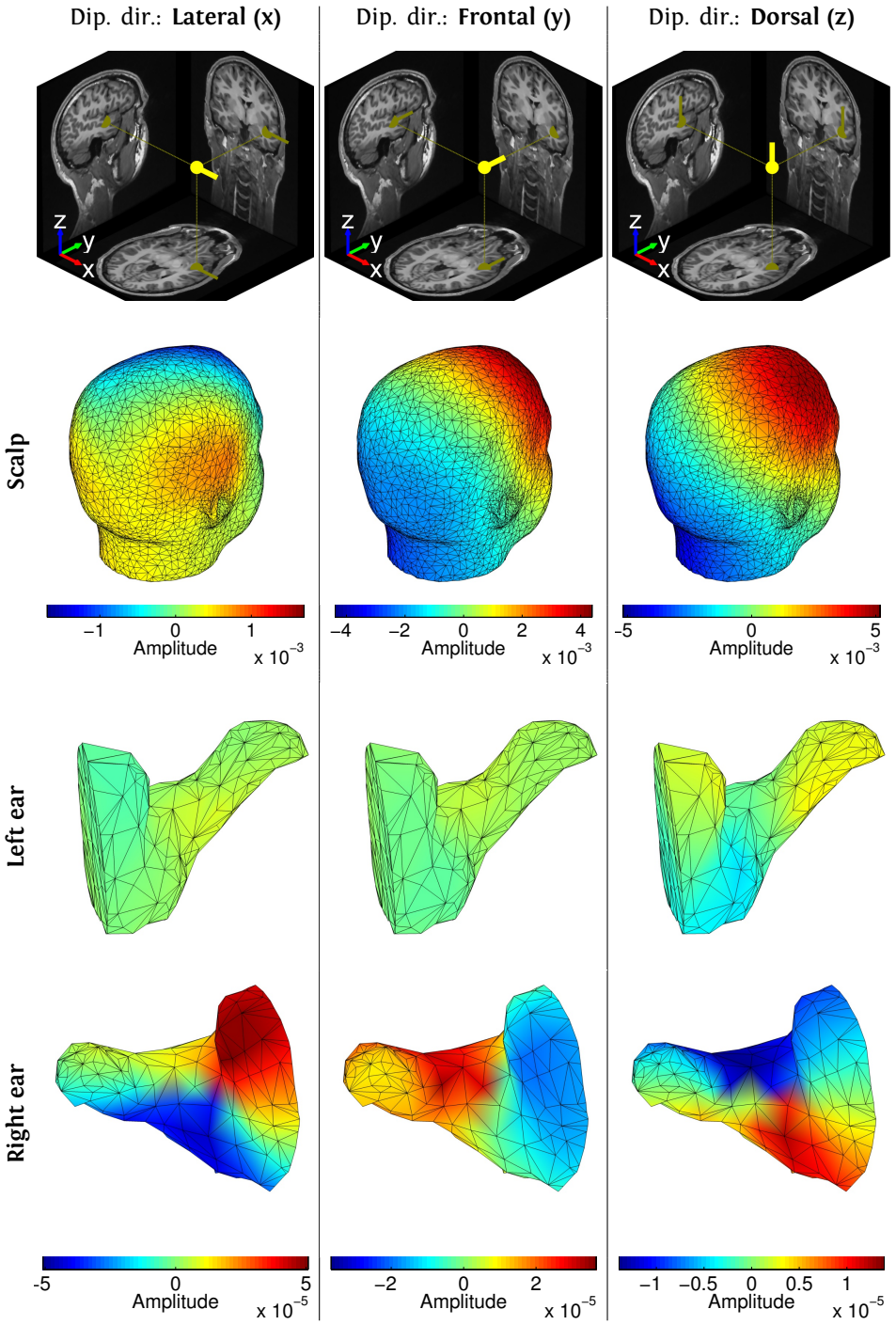

Figure 6.4: Mapping of dipoles in the right primary auditory cortex. The location and direction of the dipoles are illustrated by the plots in the top row. [Click on the 3D objects to zoom and rotate - only supported by Adobe Acrobat Reader.]

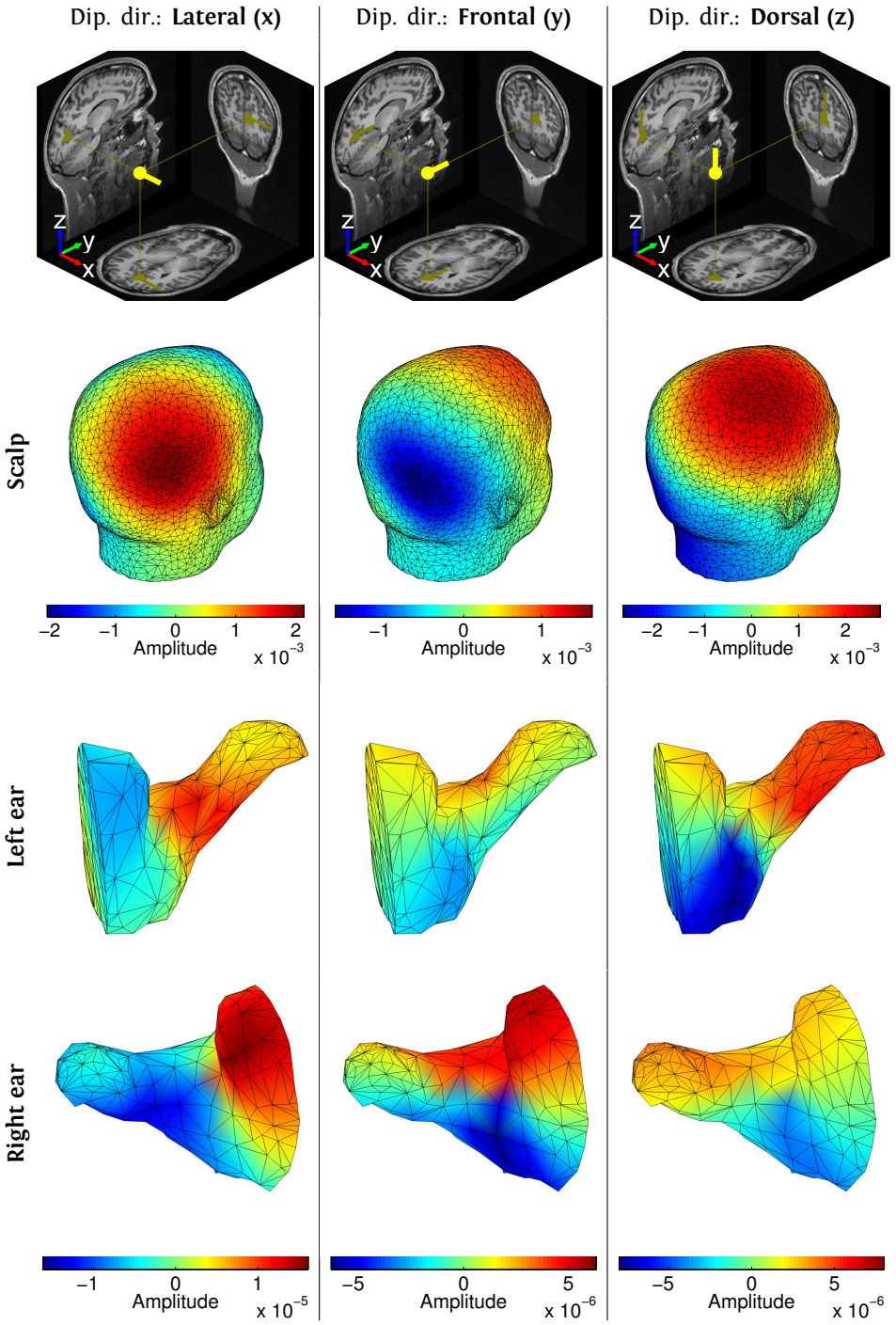

Figure 6.5: Mapping of dipoles in the right primary visual cortex. The location and direction of the dipoles are illustrated by the plots in the top row. [Click on the 3D objects to zoom and rotate - only supported by Adobe Acrobat Reader.]

Chapter 7

Conclusion and perspectives

"The future cannot be predicted, but futures can be invented."
— Dennis Gabor, Hungarian/British electrical engineer and physicist, 1963

This Ph.D. project concerned the development and characterization of ear-EEG for real-life brain-monitoring. This objective was addressed through the characterization of real-life physiological artifacts, development and characterization of dry-contact electrodes for ear-EEG, and characterization of ear-EEG based on well-established EEG paradigms in real-life settings. A method was also developed to map cortical sources to the ear, and thereby increase our understanding of the electric field propagation from brain sources to the ear.

7.1 Conclusion

The study of real-life physiological artifacts, generated in a controlled laboratory setting, showed a similar artifact level for recordings from ear electrodes and temporal lobe scalp electrodes. An early real-life study of artifacts performed with wet ear electrodes, showed that ear-EEG was less influenced by real-life artifacts than scalp EEG. The results from the artifact studies are promising for future applications of ear-EEG in the everyday life.

An important step towards improving the user-friendliness and comfort of ear-EEG devices, was the development of flexible earpieces and dry contact electrodes. The flexible earpieces were customized to the anatomical shape of the subject's ears, and the dry-contact electrodes were developed to be inserted into the earpieces. The impedance of the electrode-skin interface was characterized for the developed electrodes, and was lower and more stable than the impedance of dry-contact silver electrodes. Parallel to this project, low power electronic instrumentation was developed. The instrumentation allow implementation in a hearing-aid-sized device

for long-term monitoring of ear-EEG with dry-contact electrodes. This project provided fundamental input to the specification and validation of the instrumentation. The development of the electronic instrumentation is an example of the collaboration needed to develop an ear-EEG device featuring an earpiece, electrodes, and electronic instrumentation.

The flexible earpieces and dry-contact electrodes were tested in a study of 4 well-established paradigms, including auditory stimulation, visual stimulation and spontaneous EEG. Recordings were performed in a laboratory and real-life setting. The responses measured by temporal lobe scalp electrodes and ear electrodes were similar, when referenced to a Cz scalp electrode. However, when the reference electrode was located closer to or in the ear, the responses were less visible and more contaminated by noise. Thus, the recordings emphasize the challenges associated with performing real-life ear-EEG recordings. Further development of the earpieces and dry-contact electrodes are needed to obtain high quality real-life ear-EEG recordings, when the reference electrode is located in the ear.

A novel method for creating head models, which include the ears, was developed. The method enables calculation of an ear-EEG forward model, which describes the mapping of the electric fields from well-defined cortical sources to the scalp and ear. A forward model, created for one subject, was used to map dipoles located in right primary auditory and visual cortices to the ears and scalp. The potentials calculated with the forward model for ear and behind-the-ear electrodes corresponded well to previous ear-EEG studies.

In conclusion, the studies presented in the dissertation confirm that recordings of ear-EEG can be performed in real-life settings with dry-contact electrodes. The studied brain processes were established with comparable clarity in both temporal lobe EEG and ear-EEG recordings. With further development of the earpieces, electrodes, and electronic instrumentation it appears to be realistic to implement ear-EEG into unobtrusive and user-friendly devices for monitoring human brain processes in real-life.

7.2 Perspectives

The project was part of the bigger hypoglycemia project, described in Section 1.2. In the hypoglycemia project, the plan is to perform ear-EEG recordings of induced hypoglycemia within one year from the end of this project. These recordings will investigate whether ear-EEG can be used for detection of severe hypoglycemia (SH, insulin shock). If the results of the study are positive, this will support the development of an ear-EEG based SH alarm device.

The mapping of cortical sources to the ear, presented in Chapter 6, was the first step in establishing head models, which include the ears. Future work will focus on calculation of head models for more subjects and validation of the head

models with data collected during the stay at Swartz Center for Computational Neuroscience.

As the shape of ear-EEG devices are similar to earpieces used for hearing aids, it is natural to consider applications where ear-EEG provides neurofeedback to algorithms in hearing aids. Several aspects of hearing aids could benefit from neurofeedback; e.g. decoding of auditory attention, brain-computer interfaces (BCI), or objective hearing assessment. Hearing threshold estimation using ear-EEG is currently being explored by Christensen et al. [25]. In this context, the method for optimizing electrode configurations, presented in Section 5.2, could be utilized.

Other applications of ear-EEG, which is currently being explored, include sleep stage classification [106] and monitoring of epilepsy. 15 patients under clinical investigations for epilepsy, have been monitored with ear-EEG in an epilepsy monitoring unit at Roskilde Hospital. However, no results from this study is published at the moment.

List of Abbreviations

ABM	alpha band modulation
ADC	analog-to-digital converter
AE	active electrode
AEP	auditory evoked potential
Ag	silver
Ag/AgCl	silver-silver chloride
AOR	auditory onset response
ASIC	application specific integrated circuit
ASSR	auditory steady-state response
BCI	brain computer interface
BE	back-end
BEM	boundary element method
CMRR	common-mode rejection ratio
CSF	cerebrospinal fluid
EEG	electroencephalography
EEI	electrode-electrolyte interface
ERP	event-related potential
ICA	independent component analysis
IRN	input referred noise
IrO_2	iridium-oxide
ITR	information transfer rate
LFM	lead field matrix
MRI	magnetic resonance imaging
NFT	neuroelectromagnetic forward-modeling toolbox

ORC	optimized reference configuration
PGA	programable gain amplifier
SDM	sigma-delta modulator
SEP	somatosensory evoked potential
SH	severe hypoglycemia
SNR	signal-to-noise ratio
SNRD	SNR deterioration
SOA	stimulus-onset asynchrony
SSR	steady-state response
SSVEP	steady-state visual evoked potential
TDA	time domain averaging
TDRL	transconductance driven-right-leg
Ti	titanium
VEP	visual evoked potential

Bibliography

[P1] S. L. Kappel, D. Looney, D. P. Mandic, and P. Kidmose. "Physiological artifacts in scalp EEG and ear-EEG". In: *Biomedical Engineering Online* 16.1 (Aug. 2017), p. 103. DOI: 10.1186/s12938-017-0391-2.

[P2] a) S. L. Kappel, M. L. Rank, H. O. Toft, M. Andersen, and P. Kidmose. "Dry-Contact Electrode Ear-EEG". In: *IEEE Trans Biomed Eng* (May 2018). DOI: 10.1109/TBME.2018.2835778;
b) S. L. Kappel and P. Kidmose. "Real-Life Dry-Contact Ear-EEG". In: *Int. Conf. of the IEEE Engineering in Medicine and Biology Society (EMBC)* (July 2018).

[P3] S. L. Kappel, C. B. Christensen, K. B. Mikkelsen, and P. Kidmose. "Reference Configurations for Ear-EEG Steady-State Responses". In: *Int. Conf. of the IEEE Engineering in Medicine and Biology Society (EMBC)* (2016). DOI: 10.1109/EMBC.2016.7592018.

[P4] S. L. Kappel and P. Kidmose. "Study of Impedance Spectra for Dry and Wet EarEEG Electrodes". In: *Int. Conf. of the IEEE Engineering in Medicine and Biology Society (EMBC)* (2015), pp. 3161–3164. DOI: 10.1109/EMBC.2015.7319063.

[P5] S. L. Kappel, D. Looney, D. P. Mandic, and P. Kidmose. "A Method for Quantitative Assessment of Artifacts in EEG, and an Empirical Study of Artifacts". In: *Int. Conf. of the IEEE Engineering in Medicine and Biology Society (EMBC)* (2014), pp. 1686–1690. DOI: 10.1109/EMBC.2014.6943931.

[P6] S. L. Kappel and P. Kidmose. "A study of real-life artifacts for scalp EEG and ear-EEG". In: *unpublished* (2016).

[P7] X. Zhou, Q. Li, S. Kilsgaard, F. Moradi, S. L. Kappel, and P. Kidmose. "A Wearable Ear-EEG Recording System Based on Dry-Contact Active Electrodes". In: *Symposia on VLSI Technology and Circuits* (June 2016). DOI: 10.1109/VLSIC.2016.7573559.

[P8] Y. T. Wang, M. Nakanishi, S. L. Kappel, P. Kidmose, D. P. Mandic, Y. Wang, CK. Cheng, and TP. Jung. "Developing an Online Steady-State Visual Evoked Potential-Based Brain-Computer Interface System Using EarEEG". In: *Int. Conf. of the IEEE Engineering in Medicine and Biology Society (EMBC)* (2015), pp. 2271–2274. DOI: 10.1109/EMBC.2015.7318845.

[P9] K. B. Mikkelsen, S. L. Kappel, D. P. Mandic, and P. Kidmose. "EEG Recorded from the Ear: Characterizing the Ear-EEG Method". In: *Frontiers in Neuroscience* 9 (Nov. 2015), pp. 1–8. DOI: 10.3389/fnins.2015.00438.

[10] Z. A. Acar and S. Makeig. "Effects of forward model errors on EEG source localization". In: *Brain Topography* 26.3 (2013), pp. 378–396. DOI: 10.1007/s10548-012-0274-6.

[11] Z. A. Acar and S. Makeig. "Neuroelectromagnetic Forward Head Modeling Toolbox". In: *Journal of Neuroscience Methods* 190 (2010), pp. 258–270. DOI: 10.1016/j.jneumeth.2010.04.031.

[12] Z. Akalin-Acar and N. G Gençer. "An advanced boundary element method (BEM) implementation for the forward problem of electromagnetic source imaging." In: *Physics in medicine and biology* 49.21 (2004), pp. 5011–5028. DOI: 10.1088/0031-9155/49/21/012.

[13] V. Augustyn, P. Simon, and B. Dunn. "Pseudocapacitive oxide materials for high-rate electrochemical energy storage". In: *Energy & Environmental Science* 7.5 (Mar. 2014), pp. 1597–1614. DOI: 10.1039/c3ee44164d.

[14] J. Augustynski, M. Koudelka, J. Sanchez, and B. E. Conway. "ESCA study of the state of iridium and oxygen in electrochemically and thermally formed iridium oxide films". In: *Journal of Electroanalytical Chemistry* 160.1-2 (Jan. 1984), pp. 233–248. DOI: 10.1016/S0022-0728(84)80128-X.

[15] H. Bakardjian, T. Tanaka, and A. Cichocki. "Optimization of SSVEP brain responses with application to eight-command Brain-Computer Interface". In: *Neuroscience Letters* 469.1 (2010), pp. 34–38. DOI: 10.1016/j.neulet.2009.11.039.

[16] H. Berger. "Über das Elektrenkephalogramm des Menschen". In: *Archiv für Psychiatrie und Nervenkrankheiten* 87.1 (1929), pp. 527–570. DOI: 10.1007/BF01797193.

[17] W. Biesmans, A. Bertrand, J. Wouters, and M. Moonen. "Optimal spatial filtering for auditory steady-state response detection using high-density EEG". In: *The IEEE International Conference on Acoustics, Speech and Signal processing (ICASSP)* (2015).

[18] M. G. Bleichner, M. Lundbeck, M. Selisky, F. Minow, M. Jager, R. Emkes, S. Debener, and M. de Vos. "Exploring miniaturized EEG electrodes for brain-computer interfaces. An EEG you do not see?" In: *Physiological Reports* 3.4 (2015), e12362. DOI: 10.14814/phy2.12362.

[19] M. G. Bleichner, B. Mirkovic, and S. Debener. "Identifying auditory attention with ear-EEG: cEEGrid versus high-density cap-EEG comparison". In: *Journal of Neural Engineering* 13.6 (2016), p. 066004. DOI: 10.1088/1741-2560/13/6/066004.

[20] T. Brousse, D. Bélanger, and J. W. Long. "To Be or Not To Be Pseudocapacitive?" In: *Journal of The Electrochemical Society* 162.5 (Mar. 2015), A5185–A5189. DOI: 10.1149/2.0201505jes.

[21] R. F. Burkard and M. Don. "The Auditory Brainstem Response". In: *Auditory evoked potentials: basic principles and clinical application*. Ed. by R. F. Burkard, J. J. Eggermont, and M. Don. 2nd ed. Philadelphia, Pennsylvania, USA: Lippincott Williams & Wilkins, 2007. Chap. 11, pp. 229–253. ISBN: 9780781757560.

[22] A. J. Casson, D. Yates, D. Smith, J. S. Duncan, and E. Rodriguez-Villegas. "Wearable electroencephalography". In: *IEEE Engineering in Medicine and Biology Magazine* 29.3 (May 2010), pp. 44–56. DOI: 10.1109/memb.2010.936545.

[23] Y. M. Chi, T. P. Jung, and G. Cauwenberghs. "Dry-Contact and Noncontact Biopotential Electrodes: Methodological Review". In: *IEEE Reviews in Biomedical Engineering* 3 (Dec. 2010), pp. 106–119. DOI: 10.1109/RBME.2010.2084078.

[24] Y. M. Chi, Y. T. Wang, Y. Wang, C. Maier, T. P. Jung, and G. Cauwenberghs. "Dry and noncontact EEG sensors for mobile brain-computer interfaces". In: *IEEE Transactions on Neural Systems and Rehabilitation Engineering* 20.2 (2012), pp. 228–235. DOI: 10.1109/TNSRE.2011.2174652.

[25] C. B. Christensen and P. Kidmose. "Objective Audiometry using Ear-EEG". In: *The Second International Meeting on Internet & Audiology*. Eriksholm Research Centre, Denmark, 2015.

[26] J. W. Clark. "The Origin of Biopotentials". In: *Medical instrumentation Application and Design*. Ed. by J. G. Webster. 4th ed. Hoboken, New Jersey: John Wiley & Sons, Inc, 2009. Chap. 4, pp. 126–188. ISBN: 9780471676003.

[27] S. F. Cogan. "Neural stimulation and recording electrodes". In: *Annual review of biomedical engineering* 10 (Aug. 2008), pp. 275–309. DOI: 10.1146/annurev.bioeng.10.061807.160518.

[28] S. F. Cogan, T. D. Plante, and J. Ehrlich. "Sputtered iridium oxide films (SIROFs) for low-impedance neural stimulation and recording electrodes." In: *IEMBS '04. 26th Annual International Conference of the IEEE* 2 (2004), pp. 4153–4156. DOI: 10.1109/IEMBS.2004.1404158.

[29] B. E. Conway, V. Birss, and J. Wojtowicz. "The role and utilization of pseudocapacitance for energy storage by supercapacitors". In: *J. Power Sources* 66.1-2 (1997), pp. 1–14. DOI: 10.1016/S0378-7753(96)02474-3.

[30] B. E. Conway and W. G. Pell. "Double-layer and pseudocapacitance types of electrochemical capacitors and their applications to the development of hybrid devices". In: *Journal of Solid State Electrochemistry* 7.9 (2003), pp. 637–644. DOI: 10.1007/s10008-003-0395-7.

[31] M. de Vos, M. Kroesen, R. Emkes, and S. Debener. "P300 speller BCI with a mobile EEG system: comparison to a traditional amplifier". In: *Journal of Neural Engineering* 11.3 (June 2014). DOI: 10.1088/1741-2560/11/3/036008.

[32] S. Debener, R. Emkes, M. de Vos, and M. Bleichner. "Unobtrusive ambulatory EEG using a smartphone and flexible printed electrodes around the ear." In: *Scientific reports, Nature Publishing Group* 5 (2015), p. 16743. DOI: 10.1038/srep16743.

[33] S. Debener, F. Minow, R. Emkes, K. Gandras, and M. de Vos. "How about taking a low-cost, small, and wireless EEG for a walk?" In: *Psychophysiology* 49.11 (Nov. 2012), pp. 1617–1621. DOI: 10.1111/j.1469-8986.2012.01471.x.

[34] A. Delorme and S. Makeig. "EEGLAB: An open source toolbox for analysis of single-trial EEG dynamics including independent component analysis". In: *Journal of Neuroscience Methods* 134.1 (Mar. 2004), pp. 9–21. DOI: 10.1016/j.jneumeth.2003.10.009.

[35] N. S. Dias, J. P. Carmo, A. Ferreira Da Silva, P. M. Mendes, and J. H. Correia. "New dry electrodes based on iridium oxide (IrO) for non-invasive biopotential recordings and stimulation". In: *Sensors and Actuators A: Physical* 164.1-2 (Nov. 2010), pp. 28–34. DOI: 10.1016/j.sna.2010.09.016.

[36] J. Duun-Henriksen, R. E. Madsen, L. S. Remvig, C. E. Thomsen, H. B. Sorensen, and T. W. Kjaer. "Automatic Detection of Childhood Absence Epilepsy Seizures: Toward a Monitoring Device". In: *Pediatric Neurology* 46.5 (May 2012), pp. 287–292. DOI: 10.1016/j.pediatrneurol.2012.02.018.

[37] F. Farooq, D. Looney, D. P. Mandic, and P. Kidmose. "EarEEG based visual P300 Brain-Computer Interface". In: *7th International IEEE/EMBS Conference on Neural Engineering (NER)* (Apr. 2015), pp. 98–101. DOI: 10.1109/NER.2015.7146569.

[38] L. A. Farwell and E. Donchin. "Talking off the top of your head: toward a mental prosthesis utilizing event-related brain potentials". In: *Electroencephalography and Clinical Neurophysiology* 70.6 (1988), pp. 510–523. DOI: 10.1016/0013-4694(88)90149-6.

[39] M. Ferrari and V. Quaresima. "A brief review on the history of human functional near-infrared spectroscopy (fNIRS) development and fields of application". In: *NeuroImage* 63.2 (Nov. 2012), pp. 921–935. DOI: 10.1016/j.neuroimage.2012.03.049.

[40] P. Fiedler, S. Griebel, P. Pedrosa, C. Fonseca, F. Vaz, L. Zentner, F. Zanow, and J. Haueisen. "Multichannel EEG with novel Ti/TiN dry electrodes". In: *Sensors and Actuators, A: Physical* 221.1 (Jan. 2015), pp. 139–147. DOI: 10.1016/j.sna.2014.10.010.

[41] P. Fiedler, P. Pedrosa, S. Griebel, C. Fonseca, F. Vaz, E. Supriyanto, F. Zanow, and J. Haueisen. "Novel Multipin Electrode Cap System for Dry Electroencephalography". In: *Brain Topography* 28.5 (Sept. 2015), pp. 647–656. DOI: 10.1007/s10548-015-0435-5.

[42] E. Frackowiak and F. Béguin. "Carbon materials for the electrochemical storage of energy in capacitors". In: *Carbon* 39.6 (2001), pp. 937–950. DOI: 10.1016/S0008-6223(00)00183-4.

[43] R. Galambos, S. Makeig, and P. J. Talmachoff. "A 40-Hz auditory potential recorded from the human scalp". In: *Proceedings of the National Academy of Sciences of the USA (PNAS)* 78.4 (Apr. 1981), pp. 2643–2647. DOI: 10.1073/pnas.78.4.2643.

[44] F. A. Gibbs, H. H. Davis, and W. G. Lennox. "The electro-encephalogram in epilepsy and in conditions of impaired consciousness". In: *Archives of Neurology & Psychiatry* 34.6 (Dec. 1935), pp. 1133–1148. DOI: 10.1001/archneurpsyc.1935.02250240002001.

[45] I. I. Goncharova, D. J. McFarland, T. M. Vaughan, and J. R. Wolpaw. "EMG contamination of EEG: spectral and topographical characteristics". In: *Clinical Neurophysiology* 114.9 (Sept. 2003), pp. 1580–1593. DOI: 10.1016/S1388-2457(03)00093-2.

[46] M. Guermandi, R. Cardu, E. F. Scarselli, and R. Guerrieri. "Active electrode IC for EEG and electrical impedance tomography with continuous monitoring of contact impedance". In: *IEEE Transactions on Biomedical Circuits and Systems* 9.1 (2015), pp. 21–33. DOI: 10.1109/TBCAS.2014.2311836.

[47] U. Ha, Y. Lee, H. Kim, T. Roh, J. Bae, C. Kim, and H. J. Yoo. "A wearable EEG-HEG-HRV multimodal system with real-time tES monitoring for mental health management". In: *IEEE International Solid-State Circuits Conference* (Feb. 2015), pp. 396–397. DOI: 10.1109/ISSCC.2015.7063093.

[48] H. Hallez, B. Vanrumste, R. Grech, J. Muscat, W. De Clercq, A. Vergult, Y. D'Asseler, K. P. Camilleri, S. G. Fabri, S. Van Huffel, and I. Lemahieu. "Review on solving the forward problem in EEG source analysis." In: *Journal of neuroengineering and rehabilitation* 4 (2007), p. 46. DOI: 10.1186/1743-0003-4-46.

[49] W. F. Haupt and J. Rudolf. "European brain death codes: A comparison of national guidelines". In: *Journal of Neurology* 246.6 (1999), pp. 432–437. DOI: 10.1007/s004150050378.

[50] J. E. Huggins, P. A. Wren, and K. L. Gruis. "What would brain-computer interface users want? Opinions and priorities of potential users with amyotrophic lateral sclerosis". In: *Amyotrophic Lateral Sclerosis* 12.5 (2011), pp. 318–324. DOI: 10.3109/17482968.2011.572978.

[51] E. Huigen, A. Peper, and C. A. Grimbergen. "Investigation into the origin of the noise of surface electrodes". In: *Medical & Biological Engineering & Computing* 40.3 (May 2002), pp. 332–338. DOI: 10.1007/BF02344216.

[52] C. Iber, S. Ancoli-Israel, A. L. Chesson, and S. F. Quan. *The AASM manual for the scoring of sleep and associated events: rules, terminology and technical specifications*. Westchester, IL: American Academy of Sleep Medicine, 2007.

[53] C. B. Juhl, K. Højlund, R. Elsborg, M. K. Poulsen, P. E. Selmar, J. J. Holst, C. Christiansen, and H. Beck-Nielsen. "Automated detection of hypoglycemia-induced EEG changes recorded by subcutaneous electrodes in subjects with type 1 diabetes – The brain as a biosensor". In: *Diabetes Research and Clinical Practice* 88.1 (Apr. 2010), pp. 22–28. DOI: 10.1016/j.diabres.2010.01.007.

[54] S. Kakooei, C. Ismail, and B. Ari-Wahjoedi. "An overview of pH Sensors Based on Iridium Oxide: Fabrication and Application". In: *International Journal of Material Science Innovations (IJMSI)* 1.1 (Feb. 2013), pp. 62–72.

[55] P. Kidmose, D. Looney, M. Ungstrup, M. L. Rank, and D. P. Mandic. "A Study of Evoked Potentials From Ear-EEG". In: *IEEE Trans. Biomedical Engineering* 60.10 (Oct. 2013), pp. 2824–2830. DOI: 10.1109/TBME.2013.2264956.

[56] C. M. Lacadie, R. K. Fulbright, N. Rajeevan, R. T. Constable, and X. Papademetris. "More accurate Talairach coordinates for neuroimaging using non-linear registration". In: *NeuroImage* 42.2 (Aug. 2008), pp. 717–725. DOI: 10.1016/j.neuroimage.2008.04.240.

[57] J. H. Lee, S. M. Lee, H. J. Byeon, J. S. Hong, K. S. Park, and S. H. Lee. "CNT/PDMS-based canal-typed ear electrodes for inconspicuous EEG recording". In: *Journal of Neural Engineering* 11.4 (June 2014), p. 046014. DOI: 10.1088/1741-2560/11/4/046014.

[58] C. T. Lin, L. D. Liao, Y. H. Liu, I. J. Wang, B. S. Lin, B. S. Lin, and J. C. Chang. "Novel dry polymer foam electrodes for long-term EEG measurement". In: *IEEE Transactions on Biomedical Engineering* 58.5 (May 2011), pp. 1200–1207. DOI: 10.1109/TBME.2010.2102353.

[59] Y. P. Lin, Y. Wang, Z. P. Jung, C. Gracitelli, R. Y. Abe, S. Baig, and F. A. Medeiros. "Using Multifocal Steady-State Visual Evoked Potentials for Objective Assessment of Visual Field Loss in Glaucoma". In: *Investigative Ophthalmology & Visual Science* 56.7 (2016), p. 486.

[60] R. D. Linden, T. W. Picton, G. Hamel, and K. B. Campbell. "Human auditory steady-state evoked potentials during selective attention." In: *Electroencephalography and clinical neurophysiology* 66.2 (1987), pp. 145–159. DOI: 10.1016/0013-4694(87)90184-2.

[61] O. G. Lins, T. W. Picton, B. L. Boucher, A. Durieux-Smith, S. C. Champagne, L. M. Moran, M. C. Perez-Abalo, V. Martin, and G. Savio. "Frequency-specific audiometry using steady-state responses". In: *Ear and hearing* 17.2 (1996), pp. 81–96.

[62] D. Looney, C. Park, P. Kidmose, M. L. Rank, M. Ungstrup, K. Rosenkranz, and D.P. Mandic. "An In-The-Ear Platform For Recording Electroencephalogram". In: *Int. Conf. of the IEEE Engineering in Medicine and Biology Society (EMBC)* (2011), pp. 6882–6885. DOI: 10.1109/IEMBS.2011.6091733.

[63] S. J. Luck. "A Broad Overview of the Event-Related Potential Technique". In: *An Introduction to the Event-Related Potential Technique*. 2nd ed. Cambridge, Massachusetts, USA: The MIT Press, 2005. Chap. 1, pp. 1–34. ISBN: 9780262122771.

[64] S. J. Luck. *An Introduction to the Event-Related Potential Technique*. 2nd ed. Cambridge, Massachusetts, USA: The MIT Press, 2005. ISBN: 9780262122771.

[65] S. J. Luck. "Artifact Rejection and Correction". In: *An Introduction to the Event-Related Potential Technique*. 2nd ed. Cambridge, Massachusetts, USA: The MIT Press, 2005. Chap. 6, pp. 185–217. ISBN: 9780262122771.

[66] S. J. Luck. "Baseline Correction, Averaging, and Time-Frequency Analysis". In: *An Introduction to the Event-Related Potential Technique*. 2nd ed. Cambridge, Massachusetts, USA: The MIT Press, 2005. Chap. 8, pp. 249–282. ISBN: 9780262122771.

[67] S. J. Luck. "Overview of Common ERP Components". In: *An Introduction to the Event-Related Potential Technique*. 2nd ed. Cambridge, Massachusetts, USA: The MIT Press, 2005. Chap. 3, pp. 71–117. ISBN: 9780262122771.

[68] S. J. Luck. "The Design of ERP Experiments". In: *An Introduction to the Event-Related Potential Technique*. 2nd ed. Cambridge, Massachusetts, USA: The MIT Press, 2005. Chap. 4, pp. 119–146. ISBN: 9780262122771.

[69] D. S. Touretzky, M. C. Mozer, and M. E. Hasselmo, eds. *Independent Component Analysis of Electroencephalographic Data*. Cambridge MA, USA: MIT Press, 1996, pp. 145–151.

[70] O. N. Markand. "Alpha Rhythms". In: *Journal of Clinical Neurophysiology* 7.2 (1990), pp. 163–190. DOI: 10.1097/00004691-199004000-00003.

[71] B. A. Martin, K. L. Tremblay, and D. R. Stapells. "Principles and Applications of Cortical Auditory Evoked Potentials". In: *Auditory evoked potentials: basic principles and clinical application*. Ed. by R. F. Burkard, J. J. Eggermont, and M. Don. 2nd ed. Philadelphia, Pennsylvania, USA: Lippincott Williams & Wilkins, 2007. Chap. 23, pp. 482–504. ISBN: 9780781757560.

[72] S. A. M. Marzouk. "Improved electrodeposited iridium oxide pH sensor fabricated on etched titanium substrates". In: *Analytical Chemistry* 75.6 (Mar. 2003), pp. 1258–1266. DOI: 10.1021/ac0261404.

[73] G. Mcloughlin, S. Makeig, and M. T. Tsuang. "In search of biomarkers in psychiatry: EEG-based measures of brain function". In: *American Journal of Medical Genetics, Part B: Neuropsychiatric Genetics* 165.2 (2014), pp. 111–121. DOI: 10.1002/ajmg.b.32208.

[74] R. D. Meyer, S. F. Cogan, T. H. Nguyen, and R. D. Rauh. "Electrodeposited iridium oxide for neural stimulation and recordingelectrodes". In: *IEEE Transactions on Neural Systems and Rehabilitation Engineering* 9.1 (Mar. 2001), pp. 2–11. DOI: 10.1109/7333.918271.

[75] F. E. Musiek, J. B. Shinn, and R. E. Jirsa. "The Auditory Brainstem Response in Auditory Nerve and Brainstem Dysfunction". In: *Auditory evoked potentials: basic principles and clinical application*. Ed. by R. F. Burkard, J. J. Eggermont, and M. Don. 2nd ed. Philadelphia, Pennsylvania, USA: Lippincott Williams & Wilkins, 2007. Chap. 14, pp. 291–253. ISBN: 9780781757560.

[76] M. R. Neuman. "Biopotential Electrodes". In: *Medical instrumentation Application and Design*. Ed. by J. G. Webster. 4th ed. Hoboken, New Jersey: John Wiley & Sons, Inc, 2009. Chap. 5, pp. 189–240. ISBN: 9780471676003.

[77] C. M. Niell and M. P. Stryker. "Modulation of Visual Responses by Behavioral State in Mouse Visual Cortex". In: *Neuron* 65.4 (Feb. 2010), pp. 472–479.

[78] F. Nijboer, E. W. Sellers, J. Mellinger, M. A. Jordan, T. Matuz, A. Furdea, S. Halder, U. Mochty, D. J. Krusienski, T. M. Vaughan, J. R. Wolpaw, N. Birbaumer, and A. Kübler. "A P300-based brain-computer interface for people with amyotrophic lateral sclerosis". In: *Clinical Neurophysiology* 119.8 (2008), pp. 1909–1916. DOI: 10.1016/j.clinph.2008.03.034.

[79] J. J. S. Norton, D. S. Lee, J. W. Lee, W. Lee, O. Kwon, P. Won, S. Y. Jung, H. Cheng, J. W. Jeong, A. Akce, S. Umunna, I. Na, Y. H. Kwon, X. Q. Wang, Z. Liu, U. Paik, Y. Huang, T. Bretl, W. H. Yeo, and J. A. Rogers. "Soft, curved electrode systems capable of integration on the auricle as a persistent brain–computer interface". In: *Proceedings of the National Academy of Sciences* 112.13 (Mar. 2015), p. 201424875. DOI: 10.1073/pnas.1424875112.

[80] T. W. Picton. "Audiometry Using Auditory Steady-State Responses". In: *Auditory evoked potentials: basic principles and clinical application*. Ed. by R. F. Burkard, J. J. Eggermont, and M. Don. 2nd ed. Philadelphia, Pennsylvania, USA: Lippincott Williams & Wilkins, 2007. Chap. 21, pp. 441–462. ISBN: 9780781757560.

[81] S. K. Piper, A. Krueger, S. P. Koch, J. Mehnert, C. Habermehl, J. Steinbrink, H. Obrig, and C. H. Schmitz. "A wearable multi-channel fNIRS system for brain imaging in freely moving subjects". In: *NeuroImage* 85 (2014), pp. 64–71. DOI: 10.1016/j.neuroimage.2013.06.062.

[82] G. Plourde and T. W. Picton. "Human auditory steady-state response during general anesthesia". In: *Anesthesia and analgesia* 71.5 (1990), pp. 460–468.

[83] H. Pratt. "Sensory ERP Components". In: *The Oxford Handbook of Event-Related Potential Components*. Ed. by S. J. Luck and E. S. Kappenman. 1st ed. Oxford, Great Britain: Oxford University Press, 2011. Chap. 4, pp. 89–114. ISBN: 9780195374148. DOI: 10.1093/oxfordhb/9780195374148.001.0001.

[84] G. Rance, F. W. Rickards, L. T. Cohen, S. De Vidi, and G. M. Clark. "The automated prediction of hearing thresholds in sleeping subjects using auditory steady-state evoked potentials". In: *Ear and hearing* 16.5 (1995), pp. 499–507. DOI: 10.1097/00003446-199510000-00006.

[85] A. Rechtschaffen and A. Kales. *A Manual of Standardized Terminology, Techniques, and Scoring System for Sleep Stages of Human Subjects*. Washington DC: US Department of Health, Education, and Welfare Public Health Service - NIH/NIND, 1968.

[86] D. Regan. "Comparison of Transient and Steady-State Methods". In: *Annals of the New York Academy of Sciences* 388.1 (1982), pp. 45–71. DOI: 10.1111/j.1749-6632.1982.tb50784.x.

[87] A. C. Metting van Rijn, A. Peper, and C. A. Grimbergen. "High-quality recording of bioelectric events. Part 1. Interference reduction, theory and practice." In: *Medical & biological engineering & computing* 28.5 (Sept. 1990), pp. 389–97. DOI: 10.1007/BF02441961.

[88] S. Sanei and J. Chambers. "EEG Source Localization". In: *EEG signal processing*. Hoboken, New Jersey: John Wiley & Sons, Ltd, 2007. Chap. 5, pp. 197–218. ISBN: 9780470025819.

[89] D. M. Schneider et al. "A synaptic and circuit basis for corollary discharge in the auditory cortex". In: *Nature* 513.7517 (Sept. 2014), pp. 189–194. DOI: 10.1038/nature13724.

[90] A. Siegel and H. N. Sapru. "Auditory and Vestibular Systems". In: *Essential Neuroscience*. 2nd ed. Philadelphia, Pennsylvania, USA: Lippincott Williams & Wilkins, 2010. Chap. 17, pp. 293–310. ISBN: 9780781783835.

[91] A. Siegel and H. N. Sapru. "Essential Neuroscience". In: 2nd ed. Philadelphia, Pennsylvania, USA: Lippincott Williams & Wilkins, 2010. ISBN: 9780781783835.

[92] N. Smidt and A. Webb. *Introduction to Medical Imaging*. 1st ed. Cambridge, UK: Cambridge university press, 2010. ISBN: 9780521190657.

[93] L. S. Snogdal, L. Folkestad, R. Elsborg, L. S. Remvig, H. Beck-Nielsen, B. Thorsteinsson, P. Jennum, M. Gjerstad, and C. B. Juhl. "Detection of hypoglycemia associated EEG changes during sleep in type 1 diabetes mellitus". In: *Diabetes Research and Clinical Practice* 98.1 (2012), pp. 91–97. DOI: 10.1016/j.diabres.2012.04.014.

[94] E. Spinelli and M. Haberman. "Insulating electrodes: a review on biopotential front ends for dielectric skin-electrode interfaces". In: *Physiological measurement* 31.10 (2010), pp. 183–98. DOI: 10.1088/0967-3334/31/10/S03.

[95] R. Srinivasan, A. F. Bibi, and P. L. Nunez. "Steady-state visual evoked potentials: Distributed local sources and wave-like dynamics are sensitive to flicker frequency". In: *Brain Topography* 18.3 (Mar. 2006), pp. 167–187. DOI: 10.1007/s10548-006-0267-4.

[96] M. Stenroos, V. Mäntynen, and J. Nenonen. "A Matlab library for solving quasi-static volume conduction problems using the boundary element method". In: *Computer Methods and Programs in Biomedicine* 88.3 (2007), pp. 256–263. DOI: 10.1016/j.cmpb.2007.09.004.

[97] F. B. Vialatte, M. Maurice, J. Dauwels, and A. Cichocki. "Steady-state visually evoked potentials: Focus on essential paradigms and future perspectives". In: *Progress in Neurobiology* 90.4 (2010), pp. 418–438. DOI: 10.1016/j.pneurobio.2009.11.005.

[98] Y. T. Wang, M. Nakanishi, Y. Wang, C. S. Wei, C. K. Cheng, and T. P. Jung. "An Online Brain-Computer Interface Based on SSVEPs Measured from Non-Hair-Bearing Areas." In: *IEEE Transactions on Neural Systems and Rehabilitation Engineering* (2016). DOI: 10.1109/TNSRE.2016.2573819.

[99] Y. T. Wang, Y. Wang, C. K. Cheng, and T. P. Jung. "Developing stimulus presentation on mobile devices for a truly portable SSVEP-based BCI." In: *Int. Conf. of the IEEE Engineering in Medicine and Biology Society (EMBC)* (Jan. 2013), pp. 5271–5274. DOI: 10.1109/EMBC.2013.6610738.

[100] Y. T. Wang, Y. Wang, and T. P. Jung. "A cell-phone-based brain-computer interface for communication in daily life". In: *Journal of Neural Engineering* 8.2 (Mar. 2011), p. 025018.

[101] J. Xu, B. Busze, C. Van Hoof, K. A. A. Makinwa, and R. F. Yazicioglu. "A 15-Channel Digital Active Electrode System for Multi-Parameter Biopotential Measurement". In: *IEEE Journal of Solid-State Circuits* 50.9 (2015), pp. 2090–2100. DOI: 10.1109/JSSC.2015.2422798.

[102] J. Xu, S. Mitra, A. Matsumoto, S. Patki, C. Van Hoof, K. A. A. Makinwa, and R. F. Yazicioglu. "A wearable 8-channel active-electrode EEG/ETI acquisition system for body area networks". In: *IEEE Journal of Solid-State Circuits* 49.9 (2014), pp. 2005–2016. DOI: 10.1109/JSSC.2014.2325557.

[103] G. B. Young. "The EEG in coma". In: *Journal of Clinical Neurophysiology* 17.5 (2000), pp. 473–485. DOI: 10.1097/00004691-200009000-00006.

[104] T. O. Zander and C. Kothe. "Towards passive brain-computer interfaces: applying brain-computer interface technology to human-machine systems in general." In: *Journal of neural engineering* 8.2 (2011), p. 025005. DOI: 10.1088/1741-2560/8/2/025005.

[105] T. O. Zander, C. Kothe, S. Welke, and M. Roetting. "Utilizing Secondary Input from Passive Brain-Computer Interfaces for Enhancing Human-Machine Interaction". In: *Foundations of Augmented Cognition. Neuroergonomics and Operational Neuroscience*. Ed. by D. D. Schmorrow, I. V. Estabrooke, and M. Grootjen. Berlin, Heidelberg: Springer, 2009, pp. 759–771. ISBN: 9783642028120. DOI: 10.1007/978-3-642-02812-0_86.

[106] I. Zibrandtsen, P. Kidmose, M. Otto, J. Ibsen, and T. W. Kjaer. "Case comparison of sleep features from ear-EEG and scalp-EEG". In: *Sleep Science* (June 2016), pp. 1–4. DOI: 10.1016/j.slsci.2016.05.006.

Corrections and updates

The corrections and updates have been revised in June 2018.

Corrections

The following corrections have been made to the original Ph.D. dissertation.

Page	Section	Description
16	Section 3.1	Illustration of reference configurations have been added to Figure 3.2. Description of reference configurations have been added to the caption and text describing Figure 3.2.
16	Section 3.1	Description of reference configuration have been added to the caption and text describing Figure 3.3.
16	Section 3.1	Description of reference configurations have been added to the caption of Figure 3.4.
20	Section 3.2	Number of subjects participating in the study described in paper P6 has been added.
20	Section 3.2	Description of the reference configurations for the real-life artifact recordings have been added.
63	Bibliography	Errors in reference [19] has been corrected.

Updates

The following updates have been made to the original Ph.D. dissertation. The updates have been made to include information on published papers in the dissertation.

Page	Section	Description
5	Section 1.5	References to published papers have been updated.
63	Section 7.2	References to published papers have been updated.
67	Section P1	The description of planned revisions has been removed, and a description of and a reference to the published paper have been added.
68	Section P2	The description of planned revisions has been removed, and descriptions of and references to the published papers have been added.
68	Section P2	DOI number has been added to reference [P3].
–	–	Paper P10, "A Wearable Ear-EEG Recording System Based on Dry-Contact Active Electrodes" by Zhou et al., has been removed from the dissertation. The paper has been rejected from publication in the journal "IEEE Journal of Solid-State Circuits (JSSC)" and there are currently no publication plans for the paper.

Part II

Scientific papers

Paper P1

Physiological artifacts in scalp EEG and ear-EEG

After submission of the dissertation, paper P1 has been revised. The data analysis methods have been improved and the presentation of the results has been updated. The revised paper is published as a peer-reviewed journal paper in BioMedical Engineering OnLine.

Paper P1: S. L. Kappel, D. Looney, D. P. Mandic, and P. Kidmose. "Physiological artifacts in scalp EEG and ear-EEG". in: *Biomedical Engineering Online* 16.1 (Aug. 2017), p. 103. DOI: 10.1186/s12938-017-0391-2

Author contributions: S. L. Kappel wrote the paper, designed the experiment, and performed the data acquisition with supervision from P. Kidmose. All authors contributed with critical revisions to the paper.

Notes:

- The random overlap method, described in Section 3.1, has not been used for the data analysis published in paper P1. Instead the data have been analyzed without performing time domain averaging.

Paper P2

Laboratory and Real-Life Dry-Contact Ear-EEG Recordings

After submission of the dissertation, the content of paper P2 has been revised and published in the following two papers:
P2a) A new laboratory study of 10 subjects has been performed with the dry-contact electrode ear-EEG platform, described in Section 4.1. The new study and platform are presented in paper P2a, which is published as a peer reviewed journal paper in IEEE Transactions on Biomedical Engineering.
P2b) The real-life and laboratory dry-contact ear-EEG recordings, presented in Section 5.1, have been reanalyzed with the algorithms developed for paper P2a. The results are published in a peer-reviewed conference paper presented at the 40th International Engineering in Medicine and Biology Conference (EMBC 2018).

Paper P2:
a) S. L. Kappel, M. L. Rank, H. O. Toft, M. Andersen, and P. Kidmose. "Dry-Contact Electrode Ear-EEG". in: *IEEE Trans Biomed Eng* (May 2018). DOI: 10.1109/TBME.2018.2835778;
b) S. L. Kappel and P. Kidmose. "Real-Life Dry-Contact Ear-EEG". in: *Int. Conf. of the IEEE Engineering in Medicine and Biology Society (EMBC)* (July 2018)

Author contributions: S. L. Kappel wrote the paper, designed the experiment, and performed the data acquisition with supervision from P. Kidmose. The dry-contact ear-EEG electrodes and flexible earpieces were developed in collaboration between all the authors of the papers.

Notes:

- The impedance measurements presented in Section 4.2 are related to the study published in paper P2b. The impedance measurements presented in Section 4.2 and published in paper P2a are not based on the same dataset.
- The results presented in Section 5.1 and published in paper P2b are based on the same dataset. However, several elements of the data analysis have been

changed before publication. Most importantly, the method to calculate the signal-to-noise ratio (SNR) of the auditory steady-state response (ASSR) and steady-state visual evoked potential (SSVEP) has been changed. Therefore, the SNR values presented in Section 5.1 and published in paper P2b are different.

Paper P3

Reference Configurations for Ear-EEG Steady-State Responses

The paper presented is accepted and published as a peer-reviewed conference paper. The paper was presented orally by S. L. Kappel at EMBC 2016 in the session "Neural Sensing" (Schedule Code: FrAT13.1).

Paper P3: S. L. Kappel, C. B. Christensen, K. B. Mikkelsen, and P. Kidmose. "Reference Configurations for Ear-EEG Steady-State Responses". In: *Int. Conf. of the IEEE Engineering in Medicine and Biology Society (EMBC)* (2016). DOI: 10.1109/EMBC.2016.7592018

Author contributions: S. L. Kappel wrote the paper, implemented the method described in the paper, and analyzed the data for validation of the method with supervision from P. Kidmose. K. B. Mikkelsen performed the data acquisition. P. Kidmose, K. B. Mikkelsen and C. B. Christensen contributed with critical revisions to the paper. The method described in the paper was developed in collaboration between all of the authors.

Paper P4

Study of Impedance Spectra for Dry and Wet EarEEG Electrodes

The paper presented is accepted and published as a peer-reviewed conference paper. The paper was presented by S. L. Kappel at EMBC 2015 in the poster session "Biolelectric Sensors and Sensor Systems" (Schedule Code: ThBPoT7.1).

Paper P4: S. L. Kappel and P. Kidmose. "Study of Impedance Spectra for Dry and Wet EarEEG Electrodes". In: *Int. Conf. of the IEEE Engineering in Medicine and Biology Society (EMBC)* (2015), pp. 3161–3164. DOI: 10.1109/EMBC.2015.7319063

Author contributions: S. L. Kappel wrote the paper, designed the experiment, developed the impedance measuring equipment, performed the data acquisition, and analyzed the data with supervision from P. Kidmose.

Paper P5

A Method for Quantitative Assessment of Artifacts in EEG, and an Empirical Study of Artifacts

The paper presented is accepted and published as a peer-reviewed conference paper. The paper was presented orally by S. L. Kappel at EMBC 2014 in the session "Bioelectric Sensors and Systems" (Schedule Code: WD12.4).

Paper P5: S. L. Kappel, D. Looney, D. P. Mandic, and P. Kidmose. "A Method for Quantitative Assessment of Artifacts in EEG, and an Empirical Study of Artifacts". In: *Int. Conf. of the IEEE Engineering in Medicine and Biology Society (EMBC)* (2014), pp. 1686–1690. DOI: 10.1109/EMBC.2014.6943931

Author contributions: S. L. Kappel wrote the paper, designed the experiment, performed the data acquisition, and analyzed the data with supervision from P. Kidmose. All authors contributed with critical revisions to the paper.

Paper P6

A study of real-life artifacts for scalp EEG and ear-EEG

The paper presented is unpublished.

Paper P6: S. L. Kappel and P. Kidmose. "A study of real-life artifacts for scalp EEG and ear-EEG". in: *unpublished* (2016)

Author contributions: S. L. Kappel wrote the paper, designed the experiment, performed the data acquisition, and analyzed the data with supervision from P. Kidmose.

A Study of Real-Life Artifacts for Scalp EEG and Ear-EEG

Simon L. Kappel[1] and Preben Kidmose[1]

Abstract— **Over the past years a lot of attention have been on performing EEG recordings outside the lab in less controlled real-life settings. However, the quality of EEG recordings in the real-life are challenged by artifacts, which are difficult to control. Ear-EEG is a non-invasive wearable EEG recording methods where EEG is recorded from electrodes embedded on a customized earpiece inserted into the ear. The paper presents a study of artifacts in EEG, recorded in real-life settings outside the lab. Recordings from 3 subjects were acquired with ear-EEG and scalp EEG simultaneously. The subjects were stimulated with an auditory steady-state stimulus. The signal-to-noise ratio (SNR) of the auditory steady-state response (ASSR) were used as a quantitative measure of the artifact level in the recordings. Additionally, recordings were performed with no applied stimulus, enabling a study of spontaneous ear-EEG and scalp EEG. Comparing the SNR of the ASSR for the lab and real-life settings, a higher decrease was observed for the scalp EEG compared to the ear-EEG. Generally higher SNR values were observed for ear-EEG, corresponding to previous studies of ASSR and ear-EEG. The recordings of spontaneous EEG, showed high coherence between ear-EEG and scalp EEG for frequencies from 10 to 40 Hz, suggesting a common source of the measured electrical potential. The study suggests that ear-EEG can be used as a standalone wearable EEG device, and measure EEG with a quality that is comparable to EEG measured by standard active scalp electrodes.**

I. Introduction

Electroencephalography is a non-invasive method for measuring electrical activity in the brain. EEG is conventionally recorded in a lab setting, where the subject is asked to relax, minimize eye-blinks and eye-movements. Over the past years a lot of attention have been on performing EEG recordings outside the lab in less controlled real-life settings. To accommodate real-life recordings, a lot of focus have been on the development of wearable EEG systems, that enable the user to move freely [1] [2]. Compared to conventional EEG systems, wearable EEG systems are less obtrusive and more user-friendly, and thereby enable long-term brain monitoring in real-life settings.

Ear-EEG is a non-invasive wearable EEG recording method where EEG is recorded from electrodes embedded on a customized earpiece inserted into the ear [3] [4]. The ear-EEG device is reasonable discreet and comfortable to wear, and the ease of use and the level of inconvenience is similar to handling and wearing a hearing aid. Thereby the ear-EEG device enables recording of EEG over extended periods of time and in the users everyday life [4].

Recording of EEG in real-life is challenging because more artifacts are present and they are more difficult to control. The most significant artifacts are eye blinks, eye movements, muscle activity and motion artifacts [5]. Previous studies of artifacts have primarily focused on the characterization of the artifacts [6] [7] and algorithms for automatic detection and removal of artifacts [8] [9].

This paper presents a characterization study of artifacts recorded in real-life settings outside the lab. Recordings from 3 subjects were acquired with ear-EEG and scalp EEG simultaneously. Measurement were also performed with no applied stimulus, enabling a study of spontaneous EEG.

[1]S. L. Kappel and P. Kidmose are with Department of Engineering, Aarhus University, DK-8200 Aarhus N, Denmark.

II. Methods

In a previous study, artifacts in ear-EEG and scalp EEG were quantified by the decrease in the signal-to-noise ratio (SNR) of an auditory steady-state response (ASSR), caused by the artifact [10]. Similarly, for the current study, the subjects were stimulated with an auditory steady-state stimulus, and the artifact level were assessed through changes in the SNR of the ASSR. The quality of the spontaneous EEG recordings were quantified in terms of the coherence between scalp and ear-EEG recordings.

A. Experimental Settings

EEG were acquired in real-life settings outside the lab as described in the following section. Additionally, a single recording for each subject were performed in a lab setting. During all recordings, the subjects had their ears occluded with the ear-EEG earpieces, causing auditory stimulus from the surroundings to be limited.

The EEG was recorded at a sampling rate of 1000 Hz using six 8-channel battery powered Avatar amplifiers (EGI, USA), connected to a common TTL trigger. Based on the trigger data, the EEG data from the amplifiers were synchronized. Four amplifiers were used to record scalp EEG and two amplifiers were used to record ear-EEG.

The scalp EEG were recorded from 32 active g.LADYbird electrodes (g.tec, Austria). All scalp electrodes were referenced to the Cz electrode and the GND electrode were placed on the left chin.

The ear-EEG were recorded from passive silver electrodes embedded on the surface of custom made earpieces as described by Looney et al. [4]. 6 electrodes were embedded on each earpiece; 2 in the concha part of the ear, labeled ExA and ExB, and 4 in the ear-canal, labeled ExE, ExG, ExI, ExK. The 'x' in the labels denote the left (L) or right (R) ear. The labeling convention was defined by Kidmose et al. [3]. The ear electrodes were referenced to the ExB electrodes and the ExA electrodes were connected to the amplifiers GND.

The left earpiece, the scalp and right earpiece were connected to galvanic disconnected EEG amplifiers, and

had different reference and GND electrodes as described above. Thus, with this setup the ear-EEG is evaluated as a standalone wearable EEG device.

Prior to insertion of the earpieces, the ears were cleaned with alcohol and skin preparation gel (Nuprep Skin Prep Gel). A high viscosity conductive gel (Elefix EEG paste) was applied to the ear electrodes before insertion. 3 male subjects with no history of neurological disorders and normal audiological status aged between 27 and 42 (mean = 33) years, participated in the study.

B. Stimulus for the artifact study

The artifact study utilized a 40 Hz ASSR, which is a paradigm largely unaffected by attention, cognitive processes, habituation or fatigue, and which does not interact with the artifacts under study [11]. Furthermore, as ear electrodes have our special interest, it was natural to choose an auditory paradigm, because the auditory cortex is located close to the ear electrodes.

The auditory steady-state stimulus was white noise amplitude modulated with 40 Hz. The stimulus was presented to the subjects in both ears by hearing aid speakers (Knowles FK60011) inserted into the ear-EEG earpieces. The stimulus was presented to the subjects at a sound level well above the individual hearing threshold.

C. Processing of EEG for the artifact study

The EEG recordings for the study of real-life artifacts, were preprocessed with the EEGLAB FIR filter function "pop_eegfiltnew()" to retain frequencies between 3 and 120 Hz [12]. Additionally a 50 Hz and a 100 Hz second order IIR notch filter was applied to the EEG data.

The preprocessed data were divided into segments of 5 s duration. The start point of each segment were aligned to a 8 Hz trigger, ensuring that the ASSR had the same phase in all segments.

For each of the segments, the mean amplitude of the segment were subtracted, and the segment was discarded if the amplitude exceeded ± 100 µV for ear-EEG and ± 1000 µV for scalp EEG. The discard limits for ear-EEG were chosen 2 times higher than proposed by Mikkelsen et al. [13]. Hence, compared to lab recordings, a higher noise level of the segments were accepted. Previous studies of ASSR and ear-EEG report approximately 20 dB difference in amplitude levels of ear-EEG and scalp EEG, which were reflected in the discard limits [14] [3] [10]. Electrodes were rejected if more than 50 % of the segments were discarded.

The steady-state response were extracted by performing time domain averaging as described in [14] using 64 of the accepted segments. The SNR of the ASSR were also calculated as described in [14] with $\omega_{low} = 35$ Hz and $\omega_{high} = 45$ Hz.

D. Real-life settings

The recordings for the study of real-life artifacts were acquired in an uncontrolled environment outside the lab, in the neighborhood of Aarhus University. Additionally, reference recordings were performed in a controlled lab environment. The artifact conditions were chosen to imitate everyday situations. The study comprised 5 settings:

1) Relax in the lab: Relax while seated on a comfortable chair in the lab. The setting were included as a reference recording.

2) Walk outside: Walk with a comfortable and relaxing pace on the sidewalk of the city streets, reflecting everyday walking.

3) Walk in mall: Simulated shopping by walking in a shopping mall with a relaxed pace and stop occasionally to look a shop windows.

4) Relax in mall: Sitting relaxed on a bench in a shopping mall. The setting was similar to relaxing in the lab, but without the comfort of a chair and with an increased level of auditory and visual stimulus from the surroundings.

5) Cycling: Cycling up and down hill on a bicycle path. The setting exemplify hard physical activity with a high level of body motion and muscle activity.

E. Spontanous EEG

In addition to the EEG recordings acquired for the artifact study, EEG were recorded with no applied stimulus during walk on the sidewalk. The recordings were performed to determine the quality of spontaneous EEG recorded with ear-EEG in a real-life environment.

The scalp and ear-EEG were recorded with different amplifiers, causing the sampling rate of the recordings to be slightly different. The actual sampling rate of the data were estimated by assuming that the frequency of the power line interference (50 Hz) should be identical for all recordings. Based on the estimated sampling rates, the data were resampled to a sampling rate of 100 Hz.

The resampled data were filtered from 2 to 45 Hz using the FIR filter function implemented in the EEGLAB function "pop_eegfiltnew" [12]. Power spectrograms were calculated with a segment size of 4 s and an overlap of 3 s. The same segments were used for calculation of the coherence. The coherence calculations were based on the magnitude squared coherence method and welch method to estimate the cross and auto spectra. Hence, each segment were further divided into 20 subsegments with a size of 2 s overlapping 1.9 s.

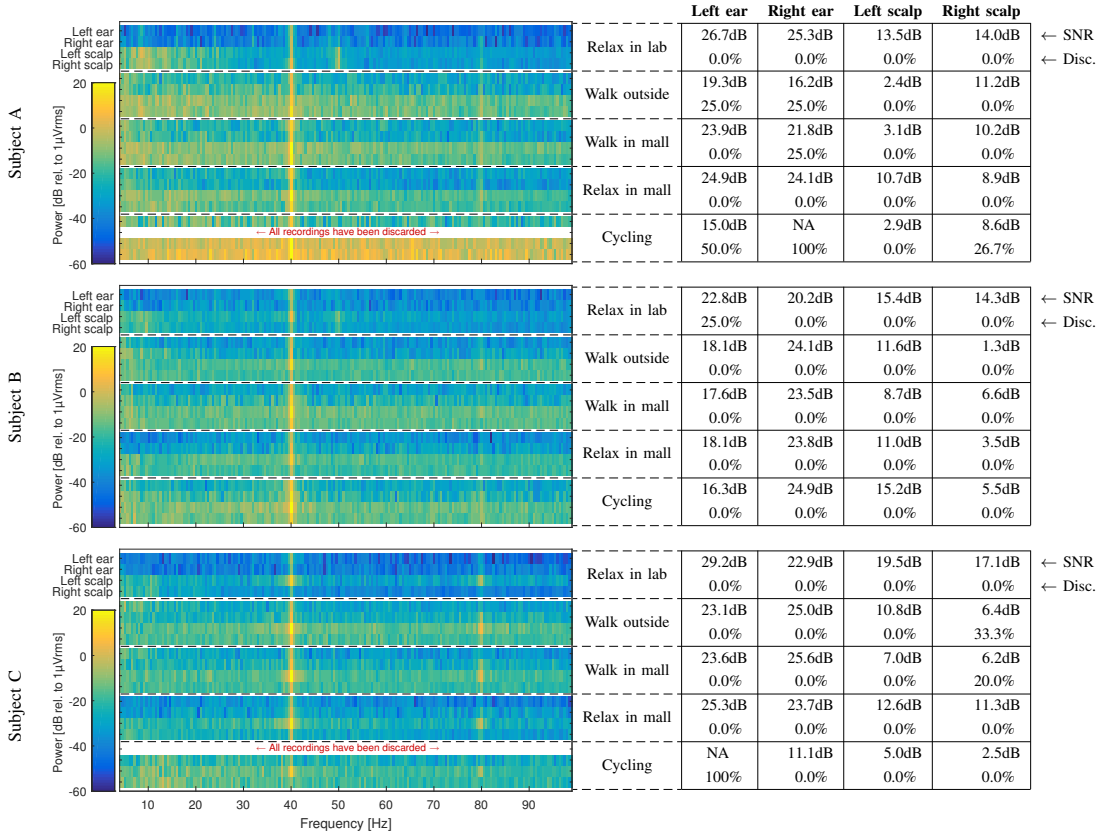

	Left ear	Right ear	Left scalp	Right scalp	
Relax in lab	26.7dB	25.3dB	13.5dB	14.0dB	← SNR
	0.0%	0.0%	0.0%	0.0%	← Disc.
Walk outside	19.3dB	16.2dB	2.4dB	11.2dB	
	25.0%	25.0%	0.0%	0.0%	
Walk in mall	23.9dB	21.8dB	3.1dB	10.2dB	
	0.0%	25.0%	0.0%	0.0%	
Relax in mall	24.9dB	24.1dB	10.7dB	8.9dB	
	0.0%	0.0%	0.0%	0.0%	
Cycling	15.0dB	NA	2.9dB	8.6dB	
	50.0%	100%	0.0%	26.7%	
Relax in lab	22.8dB	20.2dB	15.4dB	14.3dB	← SNR
	25.0%	0.0%	0.0%	0.0%	← Disc.
Walk outside	18.1dB	24.1dB	11.6dB	1.3dB	
	0.0%	0.0%	0.0%	0.0%	
Walk in mall	17.6dB	23.5dB	8.7dB	6.6dB	
	0.0%	0.0%	0.0%	0.0%	
Relax in mall	18.1dB	23.8dB	11.0dB	3.5dB	
	0.0%	0.0%	0.0%	0.0%	
Cycling	16.3dB	24.9dB	15.2dB	5.5dB	
	0.0%	0.0%	0.0%	0.0%	
Relax in lab	29.2dB	22.9dB	19.5dB	17.1dB	← SNR
	0.0%	0.0%	0.0%	0.0%	← Disc.
Walk outside	23.1dB	25.0dB	10.8dB	6.4dB	
	0.0%	0.0%	0.0%	33.3%	
Walk in mall	23.6dB	25.6dB	7.0dB	6.2dB	
	0.0%	0.0%	0.0%	20.0%	
Relax in mall	25.3dB	23.7dB	12.6dB	11.3dB	
	0.0%	0.0%	0.0%	0.0%	
Cycling	NA	11.1dB	5.0dB	2.5dB	
	100%	0.0%	0.0%	0.0%	

Fig. 1. The left part shows power spectra, with the power expressed by a color scale. Each row of the plots corresponds to a setting, and is divided in four power spectra showing averaged spectra for the left ear, right ear, left scalp and right scalp electrodes respectively. The tables to the right contain the SNR in the top of each cell and the discard percentage in the bottom of the cells.

III. Results

A. Real-life artifact conditions

In the processing of the EEG data a total of 15 (12.5 %) of the ear-EEG and 16 (3.6 %) of the scalp EEG electrodes were rejected, based on the criteria described above.

The left part of Fig. 1 shows the averaged power spectra for each of the 3 subjects and the 5 settings, averaged over the left ear, right ear, left scalp and right scalp electrodes respectively. The ASSR (response at 40 Hz) is clearly visible in the power spectra and have similar power for the scalp and ears across all artifact conditions and subjects. Because of a lower noise floor of the ear-EEG, the SNR of the ear-EEG recordings were generally higher than the SNR for the scalp EEG recordings, corresponding to previous observations for ear-EEG [3] [10]. Comparing the SNR values for the relax in lab setting with the real-life settings, a generally higher SNR deterioration were observed for the scalp electrodes, compared to the ear-EEG electrodes. For ear-EEG the SNR were similar for the relax in lab and real-life settings, with exception of cycling, where a decrease in the SNR was observed. Based on both the ear-EEG and scalp EEG recordings, it was clear that cycling generated the most severe artifacts, causing low SNR values and a high percentage of rejected ear-EEG electrodes. This corresponds well to expectations of increased muscle activity and motion required for cycling, compared to the other settings.

B. Spontanous EEG

Fig. 2 shows power and coherence spectrograms for the ERE and TP10 electrodes measured on subject A during real-life walking. Looking at the power spectrograms, similar trends is observable in the frequency range from approximately 10 to 40 Hz. This is confirmed by the coherence spectrogram in Fig 2(c) showing a high coherence for this frequency range. The high coherence suggests a common source of the electrical potential measured by the ear and scalp electrodes. It is likely that the potentials were of physiological origin, and could be electrical activity in muscles. The coherence spectrogram confirms previous observations

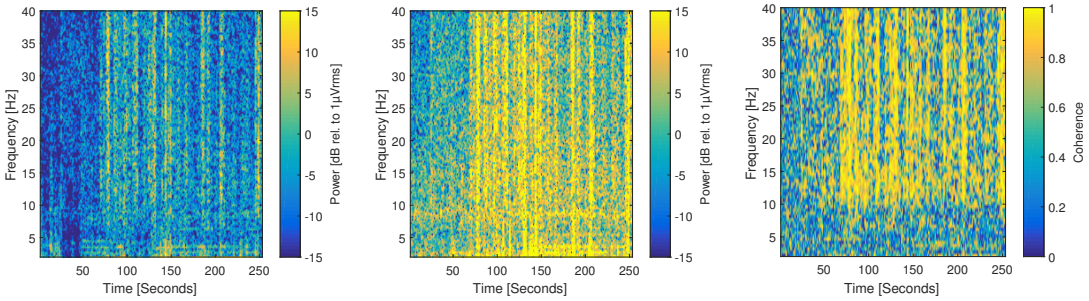

(a) Power spectrogram for ERE (b) Power spectrogram for TP10 (c) Coherence spectrogram for ERE and TP10

Fig. 2. Power and coherence spectrograms for one subject during real-life walk. (a) Power spectrogram of the ERE right ear-EEG electrode (b) Power spectrum of the TP10 scalp electrode behind the right ear (c) Spectrogram of the coherence between ERE and TP10.

of high similarity between ear-EEG and EEG from behind the ear scalp electrodes [3] [13].

IV. Conclusion

A study of artifacts for 4 real-life settings were performed. The settings were chosen to imitate everyday activities. During all recordings for the artifact characterization, the subjects were stimulated with an auditory steady-state stimulus. Artifact levels were assessed through changes in the signal-to-noise ratio (SNR) of the auditory steady-state response (ASSR). Comparing the SNR values for the lab recordings with the real-life recordings, the study generally showed a higher deterioration of the SNR for scalp EEG recordings compared to ear-EEG recordings. The SNR of the ASSR for ear-EEG recordings were generally higher than the SNR of scalp recordings. The lowest SNR values were observed during cycling, corresponding to expectations of a higher level of muscle activity and motion needed for cycling, compared to the other settings.

Additionally, EEG were acquired with no applied stimulus during real-life walk. Power spectrograms of EEG from ear and behind-the-ear electrodes showed high similarity in the EEG from 10 to 40 Hz. The similarities were reflected in the coherence spectrogram for the electrodes. The origin of the coherence between the EEG recordings was likely physiological, and could be electrical activity in muscles.

The study suggests that ear-EEG can be used as a standalone wearable EEG device, and measure EEG with a quality that is comparable to EEG from conventional active scalp electrodes.

Acknowledgment

This research was supported by the Danish National Advanced Technology Foundation (j.nr. 110-2013-1).

References

[1] Y. M. Chi, Y. T. Wang, Y. Wang, C. Maier, T. P. Jung, and G. Cauwenberghs, "Dry and noncontact EEG sensors for mobile brain-computer interfaces," *IEEE Transactions on Neural Systems and Rehabilitation Engineering*, vol. 20, pp. 228–235, 2012.

[2] A. J. Casson, D. Yates, D. Smith, J. S. Duncan, and E. Rodriguez-Villegas, "Wearable electroencephalography," *IEEE, Engineering in Medicine and Biology Magazine*, vol. 29, no. 3, pp. 44–56, 2010.

[3] P. Kidmose, D. Looney, M. Ungstrup, M. L. Rank, and D. P. Mandic, "A Study of Evoked Potentials From Ear-EEG," *IEEE Trans. Biomedical Engineering*, vol. 60, no. 10, pp. 2824–30, 2013.

[4] D. Looney, C. Park, P. Kidmose, M. L. Rank, M. Ungstrup, K. Rosenkranz, and D.P. Mandic, "An In-The-Ear Platform For Recording Electroencephalogram," *Int. Conf. of the IEEE Engineering in Medicine and Biology Society (EMBC)*, pp. 6882–6885, 2011.

[5] S. J. Luck, "A Broad Overview of the Event-Related Potential Technique," in *An Introduction to the Event-Related Potential Technique*, chapter 1, pp. 1–34. The MIT Press, Cambridge, Massachusetts, USA, 2 edition, 2005.

[6] J. C. Corby and B. S. Kopell, "Differential contributions of blinks and vertical eye movements as artifacts in EEG recording," *Psychophysiology*, vol. 9, no. 6, pp. 640–644, 1972.

[7] I. I. Goncharova, D. J. McFarland, T. M. Vaughan, and J. R. Wolpaw, "EMG contamination of EEG: spectral and topographical characteristics," *Clinical Neurophysiology*, vol. 114, no. 9, pp. 1580–1593, 2003.

[8] R. J. Croft and R. J. Barry, "Removal of ocular artifact from the EEG: a review," *Neurophysiologie Clinique/Clinical Neurophysiology*, vol. 30, no. 1, pp. 5–19, 2000.

[9] T. P. Jung, S. Makeig, C. Humphries, T. W. Lee, M. J. McKeown, I. Iragui, and T. J. Sejnowski, "Removing Electroencephalographic aretfacts by blind source seperation," *Psychophysiology*, vol. 37, no. 2, pp. 163–178, 2000.

[10] S. L. Kappel, D. Looney, D. P. Mandic, and P. Kidmose, "A method for quantitative assessment of artifacts in EEG, and an empirical study of artifacts," *36th Annual Int. Conf. of the IEEE Engineering in Medicine and Biology Society (EMBC)*, pp. 1686–1690, 2014.

[11] R. Galambos, S. Makeig, and P. J. Talmachoff, "A 40-Hz auditory potential recorded from the human scalp," *Proc. Nati. Acad. Sci. USA (PNAS)*, vol. 78, no. 4, pp. 2643–2647, 1981.

[12] A. Delorme and S. Makeig, "EEGLAB: An open source toolbox for analysis of single-trial EEG dynamics including independent component analysis," *Journal of Neuroscience Methods*, vol. 134, no. 1, pp. 9–21, 2004.

[13] K. B. Mikkelsen, S. L. Kappel, D. P. Mandic, and P. Kidmose, "EEG Recorded from the Ear: Characterizing the Ear-EEG Method," *Frontiers in Neuroscience*, vol. 9, no. November, pp. 1–8, 2015.

[14] S. L. Kappel, D. Looney, D. P. Mandic, and P. Kidmose, "Physiological Artifacts in Scalp EEG and Ear-EEG," *in preparation*, 2016.

Paper P7

A Wearable Ear-EEG Recording System Based on Dry-Contact Active Electrodes

The paper presented is accepted and published as a peer-reviewed conference paper.

Paper P7: X. Zhou, Q. Li, S. Kilsgaard, F. Moradi, S. L. Kappel, and P. Kidmose. "A Wearable Ear-EEG Recording System Based on Dry-Contact Active Electrodes". In: *Symposia on VLSI Technology and Circuits* (June 2016). DOI: 10.1109/VLSIC.2016.7573559

Author contributions: X. Zhou wrote the paper, designed and implemented the ASICs, and performed the system performance measurements with supervision from P. Kidmose and Q. Li. EEG recordings and analysis of the EEG data were performed by S. L. Kappel and P. Kidmose. All authors contributed with input to the design specifications for the developed system. All authors also contributed with critical revisions to the paper.

Paper P8

Developing an Online Steady-State Visual Evoked Potential-Based Brain-Computer Interface System Using EarEEG

The paper presented is accepted and published as a peer-reviewed conference paper. The paper was presented orally by Yu-Te Wang at EMBC 2015 in the session "Wearable Systems I" (Schedule Code: WeET20.3).

Paper P8: Y. T. Wang, M. Nakanishi, S. L. Kappel, P. Kidmose, D. P. Mandic, Y. Wang, CK. Cheng, and TP. Jung. "Developing an Online Steady-State Visual Evoked Potential-Based Brain-Computer Interface System Using EarEEG". in: *Int. Conf. of the IEEE Engineering in Medicine and Biology Society (EMBC)* (2015), pp. 2271–2274. DOI: 10.1109/EMBC.2015.7318845

Author contributions: Y. T. Wang, M. Nakanishi and S. L. Kappel wrote the paper and performed the data acquisition. Y. T. Wang and M. Nakanishi designed the experiment and analyzed the data. All authors contributed with critical revisions to the paper.

Paper P9

EEG Recorded from the Ear: Characterizing the Ear-EEG Method

The paper presented is accepted and published as a peer-reviewed journal paper.

Paper P9: K. B. Mikkelsen, S. L. Kappel, D. P. Mandic, and P. Kidmose. "EEG Recorded from the Ear: Characterizing the Ear-EEG Method". In: *Frontiers in Neuroscience* 9 (Nov. 2015), pp. 1–8. DOI: 10.3389/fnins.2015.00438

Author contributions: K. B. Mikkelsen wrote the paper, designed the experiment, performed the data acquisition, and analyzed the data, with exception of the α-attenuation experiment, where K.B. Mikkelsen and S. L. Kappel collaborated about design of the paradigm and data analysis. The work was supervised by P. Kidmose. All authors contributed with critical revisions to the paper.